

A HUBBLE SPACE TELESCOPE WFPC2 INVESTIGATION OF THE NUCLEAR MORPHOLOGY IN THE TOOMRE SEQUENCE OF MERGING GALAXIES¹

SEPO LAINÉ

SIRTF Science Center, Mail Code 220-6, California Institute of Technology, Pasadena, CA 91125;
seppo@ipac.caltech.edu

ROELAND P. VAN DER MAREL AND JÖRN ROSSA

Space Telescope Science Institute, 3700 San Martin Drive, Baltimore, MD 21218;
marel@stsci.edu, jrossa@stsci.edu

JOHN E. HIBBARD

National Radio Astronomy Observatory, 520 Edgemont Road, Charlottesville, VA 22903-2475;
jhubbard@nrao.edu

J. CHRISTOPHER MIHOS²

Department of Astronomy, Case Western Reserve University, 10900 Euclid Avenue, Cleveland, OH 44106;
hos@burro.astr.cwru.edu

TORSTEN BÖKER³

Space Telescope Science Institute, 3700 San Martin Drive, Baltimore, MD 21218;
boeker@rssd.esa.int

AND

ANN I. ZABLUDOFF

Steward Observatory, University of Arizona, 933 North Cherry Avenue, Tucson, AZ 85721-0065;
azabludoff@as.arizona.edu

Received 2003 June 16; accepted 2003 September 11

ABSTRACT

We report on the properties of nuclear regions in the Toomre sequence of merging galaxies, based on imaging data gathered with the *Hubble Space Telescope* WFPC2 camera. We have imaged the 11 systems in the proposed evolutionary merger sequence in the F555W and F814W broadband filters, and in H α +[N II] narrowband filters. The broadband morphology of the nuclear regions varies from nonnucleated starburst clumps through dust-covered nuclei to a nucleated morphology. There is no unambiguous trend in the morphology with merger stage. The emission-line morphology is extended beyond the nucleus in most cases, but centrally concentrated (within 1 kpc) emission-line gas can be seen in the four latest-stage merger systems. We have quantified the intrinsic luminosity densities and colors within the inner 100 pc and 1 kpc of each identified nucleus. We find little evidence for a clear trend in nuclear properties along the merger sequence other than a suggestive rise in the nuclear luminosity density in the most evolved members of the sequence. The lack of clear trends in nuclear properties is likely due both to the effects of obscuration and geometry, as well as the physical variety of galaxies included in the Toomre sequence.

Key words: galaxies: evolution — galaxies: formation — galaxies: interactions — galaxies: nuclei — galaxies: spiral

1. INTRODUCTION

Disk galaxy mergers are believed to be responsible for triggering a variety of global and nuclear responses in galaxies. The global effects have been well documented, both with observations, starting with Zwicky's extensive work (1950, 1956, 1964), and with numerical simulations, first convincingly demonstrated by Toomre & Toomre (1972). Work during the last decades strongly suggests that a fraction of elliptical galaxies have formed as a result of disk galaxy merging (see Schweizer 1998 and references therein). The morphology of tidal tails has been used to trace the

mass distribution in galactic halos (Dubinski, Mihos, & Hernquist 1996; Mihos, Dubinski, & Hernquist 1998; Springel & White 1999), and the tails themselves are possible birthplaces of some dwarf galaxies (Barnes & Hernquist 1992; Elmegreen, Kaufman, & Thomasson 1993; Duc & Brinks 2001). Mergers have also been closely connected to luminous and ultraluminous infrared galaxies (Lonsdale, Persson, & Matthews 1984; Joseph & Wright 1985; Schweizer 1990; Sanders et al. 1988a; Scoville et al. 2000; Borne et al. 2000).

Perhaps the most dramatic physical process associated with disk galaxy merging is the inflow of gas into the nuclear region and the consequent excitation of nuclear starburst and AGN activity. This process has been reported from simulations (Barnes & Hernquist 1991; Mihos & Hernquist 1994a; Barnes & Hernquist 1996) and from observations (Joseph & Wright 1985; Sanders et al. 1988a; Hutchings & Neff 1992; Bahcall, Kirhakos, & Schneider 1995; Surace, Sanders, & Evans 2001). Whether the gas "hangs up" and forms stars in the inner kiloparsec or continues to flow

¹ Based on observations with the NASA/ESA *Hubble Space Telescope*, obtained at the Space Telescope Science Institute, which is operated by the Association of Universities for Research in Astronomy, Inc., under NASA contract NAS 5-26555. These observations are associated with proposal 8669.

² NSF Career Fellow and Research Corporation Cottrell Scholar.

³ On assignment from the Space Telescope Division of the European Space Agency. Current address: Astrophysics Division, RSSD, European Space Agency, ESTEC, NL-2200 AG Noordwijk, Netherlands.

inward toward a putative AGN has a strong impact on the luminosity and evolution of the merger. The details of the nuclear gasdynamics will depend on the structure of the host galaxies and the dynamical stage of the interaction (Mihos & Hernquist 1996; Barnes & Hernquist 1996). Several scenarios have been suggested in which interactions evolve from starburst-dominated to AGN-dominated regimes as the galaxies merge (Weedman 1983; Sanders et al. 1988a; Veilleux et al. 1995).

Unfortunately, until now, both observations and numerical simulations have lacked the spatial resolution needed to study the evolution of the merging nuclei on scales smaller than a few hundred parsecs. For this reason, our understanding of how mergers fuel nuclear starburst and AGN activity, and how they drive galaxy evolution from the nucleus out, has remained woefully incomplete. Theoretical arguments suggest that the evolution of the merging nuclei is where the merger hypothesis for the formation of elliptical galaxies through disk galaxy mergers faces its most stringent test.

A wide variety of physical processes may shape the nuclei. Purely stellar dynamical merging alone would tend to produce diffuse nuclei with large cores and a very shallow nuclear surface brightness gradient (Hernquist 1992) unless the progenitor nuclei were dense (Barnes 1988). In the case of gas-rich disk galaxies the dissipative flow of gas into the nuclei and accompanying star formation would tend to result in a steep luminosity profile (Mihos & Hernquist 1994b) and a large central density, as seen in several young merger remnants (van der Marel et al. 2003; see also Fig. 2 in van der Marel & Zurek 2000). The presence of a central supermassive black hole would also induce a strong nuclear power-law cusp (Young 1980; Quinlan, Hernquist, & Sigurdsson 1995). Yet, if both galaxies contain supermassive central black holes that merge, the resulting black hole binary would act as a dynamical slingshot and eject stars from the center, thus lowering the stellar density there (Quinlan & Hernquist 1997; Milosavljević & Merritt 2001).

For these reasons we are undertaking a high-resolution *Hubble Space Telescope* (*HST*) survey of the nuclear regions in a sequence of merging galaxies. The questions we want to answer include the following: (1) What is the morphology of the ionized gas distribution around the nucleus? Is it clumpy, diffuse and extended, ringlike, or compact and disk-like? Does this morphology depend on the interaction stage? (2) How is the current star formation, as revealed by the H α line emission, distributed with respect to the young stellar populations, as revealed by their blue color (and, eventually, spectra)? (3) How do the nuclear starbursts affect the radial color gradients of the merger remnants? The spatial resolution of the *HST* (10–50 pc in nearby systems) is required to investigate these questions, which are the focus of the current paper. In future papers we will study the stellar populations, kinematics, and evolution of the merger-induced starbursts of the Toomre sequence nuclei, using *HST* Space Telescope Imaging Spectrograph (STIS) spectra and Near Infrared Camera and Multiobject Spectrometer (NICMOS) imaging.

2. GALAXY SAMPLE AND OBSERVATIONS

2.1. Sample

The Toomre sequence (Toomre 1977) is a sample of 11 relatively nearby (within \sim 120 Mpc) interacting and

merging disk galaxies, which have been arranged into a sequence according to the *putative* time before or since merging. These systems were chosen because they exhibit conspicuous tidal tails and “main bodies that are nearly in contact or perhaps not even separable” (Toomre 1977). They span a range of dynamical phases, from galaxies early in the merging process (e.g., NGC 4038/39 and NGC 4676) to late-stage merger remnants (e.g., NGC 3921 and NGC 7252; see Fig. 1 and Table 1). We want to emphasize the word *putative*, since the placing of a system in this sequence was based on the apparent degree of coalescence of the progenitor main bodies in low-resolution optical photographic plates, assuming that the progenitors resembled normal disk galaxies in the preencounter stage.

Because of the requirement of well-developed tidal tails, these systems have suffered, or are suffering, encounters that are most likely of prograde sense (with the disks rotating in the same sense as they orbit each other). In such a scenario the orbits of interacting galaxies decay as the galaxies lose orbital energy and angular momentum via dynamical friction with their dark halos. Ultimately, the galaxies coalesce and form a single merger remnant. On these grounds we can call the Toomre sequence an evolutionary sequence. Because it is an *optically* selected sample of merging galaxies, it suffers less from dust obscuration than infrared-luminous samples, allowing the nuclei to be studied at optical wavelengths. The Toomre sequence has been widely investigated by ground-based observations (Joseph & Wright 1985; Stanford & Bushouse 1991; Hibbard & van Gorkom 1996; Schweizer 1998; Georgakakis, Forbes, & Norris 2000; Yun & Hibbard 2001), space-based observations (Fabbiano, Schweizer, & Mackie 1997; Read & Ponman 1998; Awaki, Matsumoto, & Tomida 2002; Zezas et al. 2002a; Zezas et al. 2002b), and numerical studies (Toomre & Toomre 1972; Barnes 1988; Stanford & Balcells 1991; Mihos, Bothun, & Richstone 1993; Hibbard & Mihos 1995; Barnes 1998).

2.2. Observations and Data Reduction

All images were taken with the WFPC2 camera on board the *HST*. We used the F555W and F814W filters, which mimic the better known *V*- and *I*-bands, with integration times of 320 s in each band, split into two exposures of 160 s to allow for cosmic-ray rejection (see Table 2 for more information on the exposure times). Images in these bands for NGC 4038/39 (Whitmore et al. 1999), NGC 3921 (Schweizer et al. 1996), and NGC 7252 (Miller et al. 1997) already existed in the *HST* archive. We used those images in our current study. Narrowband images covering the H α +[N II] lines were taken with the F673N narrowband filter in cases where the line emission from the target fell within the wavelength range covered by this filter (NGC 3509, NGC 7592), or otherwise with the linear ramp filter (LRF). The LRFs have a bandwidth of about 1.3% of the central wavelength. The position of the galaxy on the CCD chip depends on the central wavelength and limits the field of view to about $10'' \times 10''$ for the LRF. The list of the adopted filters, central wavelengths, and FWHM values of the filters, together with integration times, are given in Table 2. The Antennae, NGC 4038/39, was imaged earlier in the *HST* F658N H α filter by Whitmore et al. (1999), and we used these data in our work.

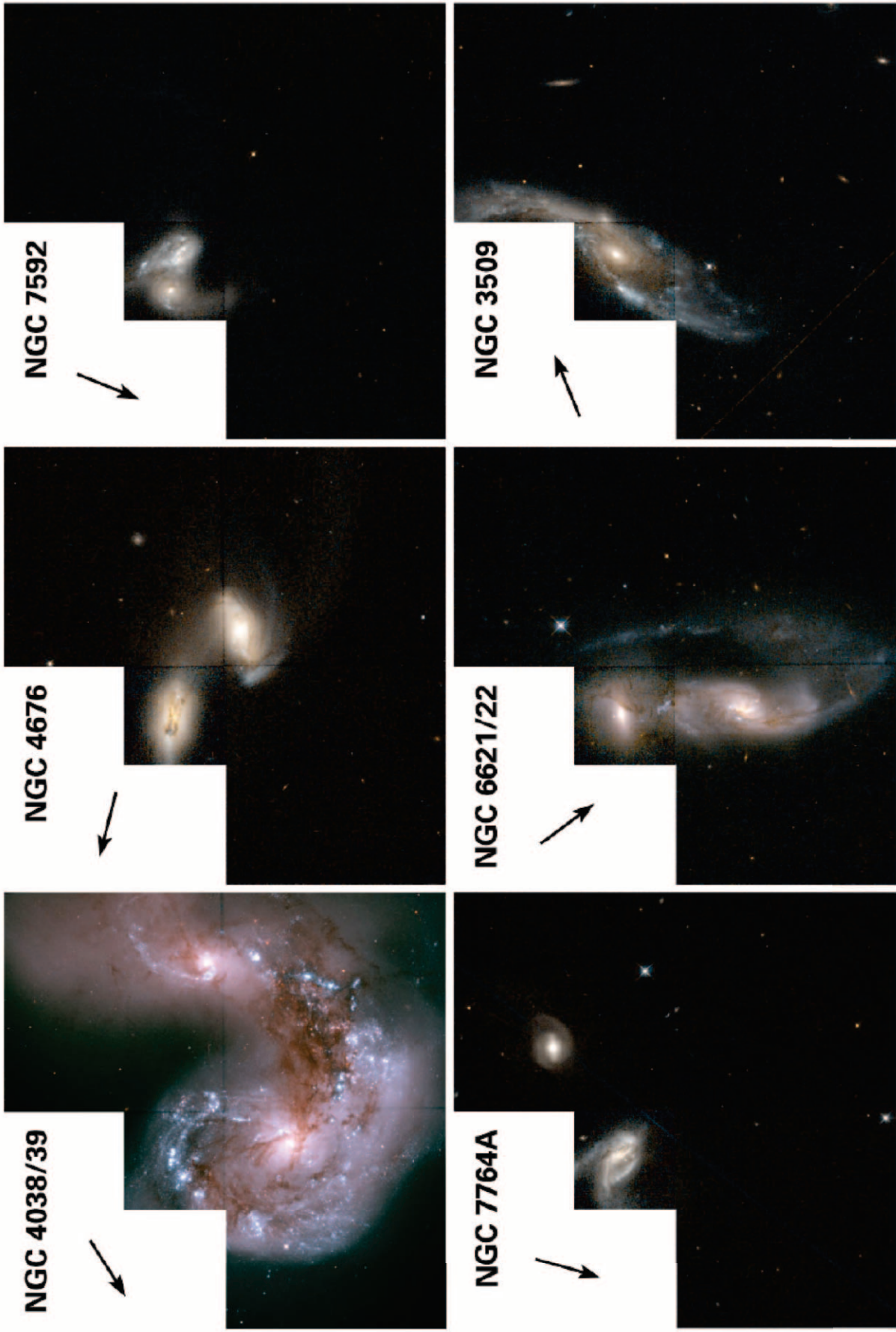


FIG. 1.—Color composite, mosaicked F555W- and F814W-band images of the Toomre sequence of merging galaxies, ordered from top left to bottom right in the original order of Toomre (1977). The arrow in each subpanel indicates the north direction. The visible trails in the NGC 7764A and NGC 3509 images are most probably satellite tracks.

FIG. 1.—*Continued*

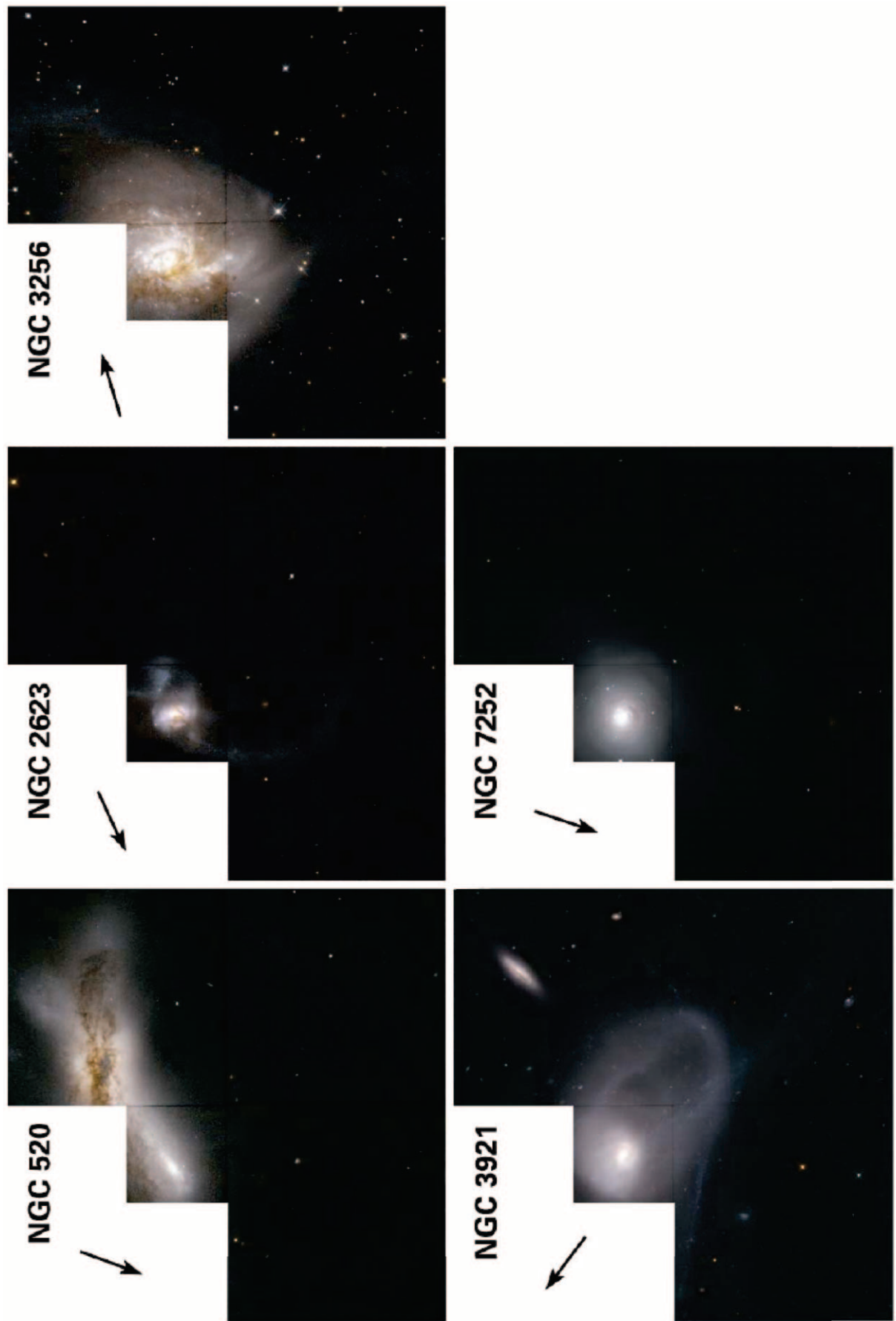


TABLE 1
THE TOOMRE SEQUENCE

Sequence Number	Galaxy	R.A. (J2000.0) ^a	Decl. (J2000.0) ^a	cz^b (km s ⁻¹)	Dist. ^c (Mpc)	θ_{nuc}^d (arcsec)	$0''1^e$ (pc)	Dynamical Model ^f
1.....	NGC 4038	12 01 53.06	-18 52 01.3	1616	21.6	61.4	10	Y ^g
1.....	NGC 4039	12 01 53.54	-18 53 09.3	1624	21.6	61.4	10	Y ^g
2.....	NGC 4676 NUC1	12 46 10.06	+30 43 55.5	6613	88.2	37.1	43	Y ^h
2.....	NGC 4676 NUC2	12 46 11.17	+30 43 21.2	6613	88.2	37.1	43	Y ^h
3.....	NGC 7592 NUC1	23 18 21.73	-04 24 56.7	7280	97.1	13.0	47	N
3.....	NGC 7592 NUC2	23 18 22.60	-04 24 57.3 ⁱ	7280	97.1	13.0	47	N
4.....	NGC 7764A	23 53 23.74	-40 48 26.3	9162	122.2	0	59	N
5.....	NGC 6621	18 12 55.25	+68 21 48.5	6191	84.4	41.7	41	N
5.....	NGC 6622	18 12 59.74	+68 21 15.1	6466	84.4	41.7	41	N
6.....	NGC 3509	11 04 23.59	+04 49 42.4	7704	102.7	0	50	N
7.....	NGC 520 NUC1	01 24 34.89	+03 47 29.9	2281	30.4	40.3	15	Y ^j
7.....	NGC 520 NUC2	01 24 33.30	+03 48 02.4	2281	30.4	40.3	15	Y ^j
8.....	NGC 2623	08 38 24.11	+25 45 16.6	5535	73.8	0	36	N
9.....	NGC 3256	10 27 51.17	-43 54 16.1	2738	36.5	0	18	N
10.....	NGC 3921	11 51 06.96	+55 04 43.1	5838	77.8	0	38	N
11.....	NGC 7252	22 20 44.78	-24 40 41.8	4688	62.5	0	30	Y ^k

NOTE.—Units of right ascension are hours, minutes, and seconds, and units of declination are degrees, arcminutes, and arcseconds.

^a Coordinates refer to the measured positions of the nuclei in our WFPC2 images, except for Nuc 1 in NGC 520 where it was measured from a ground-based *K*-band image (no clear nuclear position could be determined in our *HST* images).

^b Heliocentric velocity, data taken from NED, except for NGC 4676, for which the value was taken from the Lyon Extragalactic Database (LEDA).

^c Distance for $H_0 = 75 \text{ km s}^{-1} \text{ Mpc}^{-1}$. In cases where the two components have different systemic velocities, the distance to both is the average of the two Hubble law distances.

^d Nuclear separation in arcseconds, calculated from the listed positions.

^e Spatial scale in parsecs corresponding to 0''.1.

^f Dynamical model means that an *N*-body simulation that tries to reproduce the observed structure and kinematics of the merger exists.

^g From Barnes 1988.

^h From Barnes 1998.

ⁱ The position of Nuc 2 in NGC 7592 is highly uncertain, as it is very difficult to determine the location of the nucleus in the optical images.

^j From Stanford & Balcells 1991.

^k From Hibbard & Mihos 1995.

We employed the STSDAS task WFIXUP to interpolate (in the *x*-direction) over bad pixels as identified in the data quality files. We also used the STSDAS task WARMPIX to correct consistently warm pixels in the data, using the most recent warm pixel tables. The STSDAS task CRREJ was used to combine the two 160 s exposures. This step corrects most of the pixels affected by cosmic rays in the combined image. In general, a few cosmic rays remain uncorrected, mostly when the same pixel was hit in both exposures. Also, a small number of hot pixels remain uncorrected because they are not listed even in the most recent warm pixel tables. We corrected these with the IRAF task COSMICRAYS, setting the THRESHOLD and FLUXRATIO parameters to values selected by a careful comparison of the images before and after correction, to ensure that only questionable pixels were replaced. The rest of the reduction was done with the standard WFPC2 pipeline tasks using the best reference files available. The LRF exposures were flat-fielded using the narrowband F656N and F673N (which-ever was closer in wavelength) flat fields. We also created mosaicked F555W and F814W images with the IRAF/STSDAS task WMOSAIC. Color composite mosaics of these images, which show the environment around the nuclei, and tidal tails in some systems are displayed in Figure 1.

The photometric calibration and conversion to Johnson *V* and *I* bands was performed according to guidelines in Holtzman et al. (1995). A *K*-correction has not been applied to any of our measurements. Since the throughput of the narrowband filters does not vary much at the wavelengths

of the lines, it was possible to calibrate the line fluxes by assuming zero width for the lines (monochromatic). We used the IRAF/STSDAS SYNPHOT task BANDPAR to compute the conversion from counts per second to ergs s⁻¹ cm⁻². The results were the same within errors to those produced by the SYNPHOT task CALCPAR.

Using the known relative orientation of the various chips on WFPC2, we rotated the chips that contained the line emission and the PC-chip *V* and *I* images to the same orientation. We used stars in the images to register the frames. The final emission-line images were constructed by accounting for the different scales of images on various chips (usually the PC chip and WF2 chip) and scaling down the *V*- and *I*-band images to the expected count levels corresponding to the wavelength and band of the line image with the help of the WFPC2 exposure time calculator. We then combined the broadband images by taking their geometric mean and performed a final adjustment to this combined continuum image by selecting areas well outside emission-line regions (with pure stellar emission) and comparing fluxes in corresponding areas in the continuum and line images. Finally, we subtracted the scaled continuum image from the line image. Using the combination of *V* and *I* images eliminates the extinction terms in the case of foreground extinction, as explained in detail by Verdoes Kleijn et al. (1999). In some cases, the residual image shows negative pixels, which are most likely due to strong color gradients near the nuclei. We estimate that the final uncertainty in the line fluxes is no better than 50%, based on

TABLE 2
WFPC2 EXPOSURES WITH THE CORRESPONDING CHIP ON WHICH THE NUCLEI ARE
CENTERED AND INTEGRATION TIMES

Object	Chip	Filter	λ_0^a	$\Delta\lambda^b$	t^c (s)
NGC 4038/39 ^d	WF2/WF4	F555W	5407	1223	4×1100
NGC 4038/39 ^d	WF2/WF4	F814W	5407	1223	4×500
NGC 4038/39 ^d	WF2/WF4	F658N	6591	28.5	3800
NGC 4676 Nuc 1.....	PC1	F555W	5407	1223	2×160
NGC 4676 Nuc 1.....	PC1	F814W	7940	1758	2×160
NGC 4676 Nuc 1.....	WF2	LRF	6715.3	80.1	2×600
NGC 4676 Nuc 2.....	PC1	F555W	5407	1223	2×160
NGC 4676 Nuc 2.....	PC1	F814W	7940	1758	2×160
NGC 4676 Nuc 2.....	WF2	LRF	6714.4	79.9	2×600
NGC 7592.....	PC1	F555W	5407	1223	2×160
NGC 7592.....	PC1	F814W	7940	1758	2×160
NGC 7592.....	WF2	F673N	6732	47.2	2×600
NGC 7764A.....	PC1	F555W	5407	1223	2×160
NGC 7764A.....	PC1	F814W	7940	1758	2×160
NGC 7764A.....	WF2	LRF	6770.8	84.2	2×600
NGC 6621.....	PC1	F555W	5407	1223	2×160
NGC 6621.....	PC1	F814W	7940	1758	2×160
NGC 6621.....	WF2	LRF	6706.2	79.3	2×700
NGC 6622.....	PC1	F555W	5407	1223	2×160
NGC 6622.....	PC1	F814W	7940	1758	2×160
NGC 6622.....	WF2	LRF	6711.5	79.9	2×700
NGC 3509.....	PC1	F555W	5407	1223	2×160
NGC 3509.....	PC1	F814W	7940	1758	2×160
NGC 3509.....	PC1	F673N	6732	47.2	2×600
NGC 520 Nuc 1	PC1	F555W	5407	1223	2×160
NGC 520 Nuc 1	PC1	F814W	7940	1758	2×160
NGC 520 Nuc 1	PC1	LRF	6619.2	75.5	2×600
NGC 520 Nuc 2	PC1	F555W	5407	1223	2×160
NGC 520 Nuc 2	PC1	F814W	7940	1758	2×160
NGC 520 Nuc 2	PC1	LRF	6617.1	75.8	2×600
NGC 2623.....	PC1	F555W	5407	1223	2×160
NGC 2623.....	PC1	F814W	7940	1758	2×160
NGC 2623.....	WF2	LRF	6691.4	78.6	2×600
NGC 3256 Nuc 1.....	PC1	F555W	5407	1223	2×160
NGC 3256 Nuc 1.....	PC1	F814W	7940	1758	2×160
NGC 3256 Nuc 1.....	WF2	LRF	6631.4	75.9	2×600
NGC 3256 Nuc 2.....	PC1	F555W	5407	1223	2×160
NGC 3256 Nuc 2.....	PC1	F814W	7940	1758	2×160
NGC 3256 Nuc 2.....	WF2	LRF	6631.4	75.9	2×600
NGC 3921 ^e	PC1	F555W	5407	1223	2×1200
NGC 3921 ^e	PC1	F814W	7940	1758	2×900
NGC 3921.....	WF2	LRF	6698.9	79.0	$2 \times 700 + 800$
NGC 7252 ^f	PC1	F555W	5407	1223	3600
NGC 7252 ^f	PC1	F814W	7940	1758	2400
NGC 7252.....	WF2	LRF	6673.9	77.9	$2 \times 700 + 600$

^a Central wavelength in angstroms (from the WFPC2 Handbook, Table 3.1, Biretta et al. 2000, for the standard filters; as specified in the observations for the LRF filters).

^b Filter width in angstroms (from the WFPC2 Handbook, Table 3.1, Biretta et al. 2000, for the standard filters; equivalent Gaussian FWHM from the IRAF CALCPHOT task for the LRF filters).

^c Integration time.

^d Data from Whitmore et al. 1999.

^e Data from Schweizer et al. 1996.

^f Data from Miller et al. 1997.

varying the scaling of the continuum image within acceptable limits and comparing the derived total line fluxes.

Color index images were created by dividing the F555W image by the F814W image, taking the logarithm of the result, and correcting for differences in the color terms using the synthetic calibration from Holtzman et al. (1995). For

our new imagery (i.e., all systems except NGC 4038/39, 3921, and 7252), many regions in the raw color index images are of low signal-to-noise ratio (S/N). We therefore constructed smoothed color index maps using an adaptive filtering procedure, as described by Scoville et al. (2000), where areas with lower S/Ns were smoothed by a larger boxcar. These images were then masked so as to only show

areas with adequate signal-to-noise (S/N greater than 2 in both V and I images after being smoothed with an 11×11 pixel boxcar median filter). The resulting smoothed color index images, together with the unsmoothed broadband images and $H\alpha + [\text{N II}]$ images, are shown in Figures 2–16.

3. GALAXY MORPHOLOGY

In the following we give a brief description of each system based on Figures 2–16, together with a few references to earlier work. We use a Hubble constant of $H_0 = 75 \text{ km s}^{-1} \text{ Mpc}^{-1}$ throughout this paper.

3.1. NGC 4038 and NGC 4039 (*The Antennae*)

Perhaps the best-known system in the sequence is the Antennae. We use the spectacular *HST* V , I , and $H\alpha$ images of this system from Whitmore et al. (1999; see also Whitmore & Schweizer 1995 and Fig. 1). These images show the chaotic dust lanes and prevalent star formation in the interface between the two galaxies. They also reveal the redder color of the underlying population in the bulge component of each galaxy. The focus of the

Whitmore et al. papers was on the abundant young star clusters that have apparently formed as the result of the interaction of the two galaxies. The properties and evolution of such clusters in a merger event have been discussed extensively in a series of papers by Whitmore and his collaborators (e.g., Whitmore & Schweizer 1995; Schweizer et al. 1996; Miller et al. 1997; Whitmore et al. 1997, 1999; Zhang, Fall, & Whitmore 2001). The nuclear regions of merging galaxies are potential formation sites of new super-star clusters (Bekki & Couch 2001). We instead investigate the morphology and star formation activity in the central few hundred parsecs.

The nuclear region of the northern component of the Antennae, NGC 4038, is bracketed by star clusters in the V and I images. The position of the nucleus is most likely near the knot “J” in the classification scheme of Whitmore & Schweizer (1995) and close to the nuclear position identified in the radio continuum by Zhang et al. (2001; using the radio continuum data of Neff & Ulvestad 2000) and in the near-infrared by Mengel et al. (2001). In our I -band image this is located near the center of the frame displayed in Figure 2. There we see an elongated ringlike structure, with

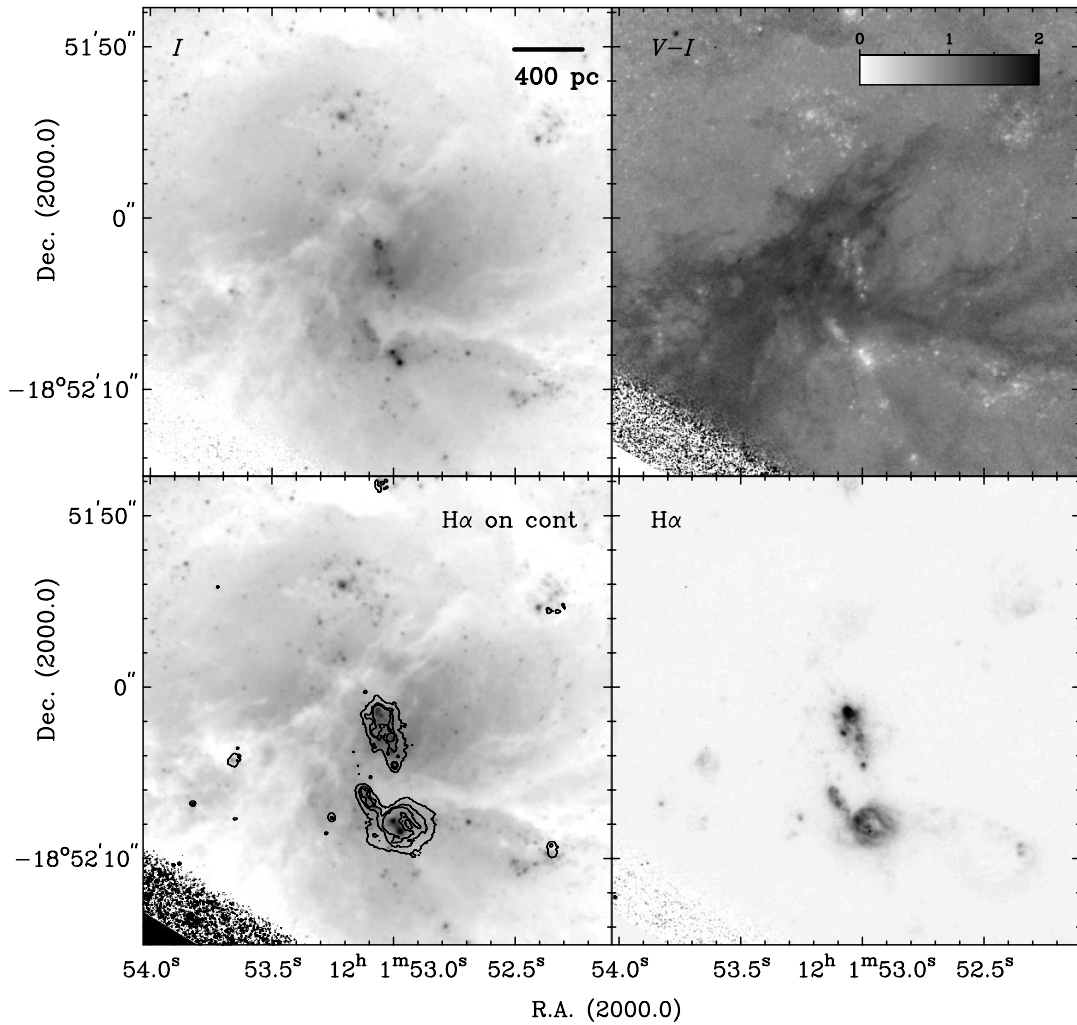


FIG. 2.—NGC 4038. *Top left:* I image. *Top right:* $V-I$ color index image. *Bottom left:* continuum (gray-scale) and $H\alpha + [\text{N II}]$ (contours) image. *Bottom right:* $H\alpha$ gray-scale image. The gray-scale levels are arbitrary and were adjusted to show details in the nuclear region. The $H\alpha$ contour levels in the bottom left image are at 10%, 30%, and 50% of $7.2 \times 10^{-17} \text{ ergs s}^{-1} \text{ cm}^{-2} \text{ pixel}^{-1}$. North is up, and east is to the left in this and in the subsequent galaxy images.

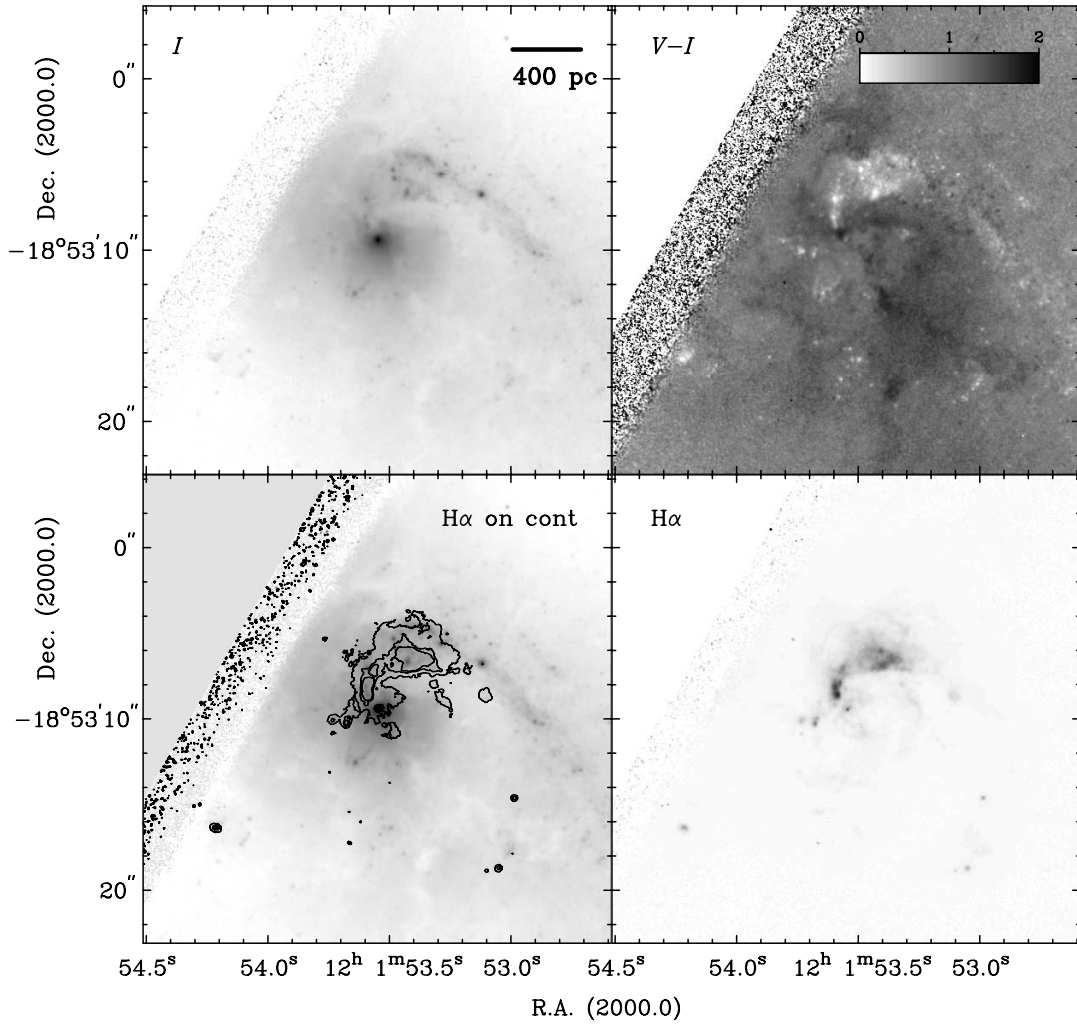


FIG. 3.—NGC 4039, as in Fig. 2. The $H\alpha$ contour levels in the bottom left image are at 10%, 30%, and 50% of $7.5 \times 10^{-17} \text{ ergs s}^{-1} \text{ cm}^{-2} \text{ pixel}^{-1}$.

an axis ratio of about 0.3 and a diameter of about $2''.5$ (260 pc), pointing north-northeast. The coordinates of the optical knot that we identified as the nucleus of NGC 4038 in the WFPC2 images are given in Table 1. They agree with the radio continuum position to within $1''$, and they are within about $3''$ of the estimated near-infrared position of the nucleus. The absolute accuracy of the coordinates reported in this paper is $\sim 1''$. This is the intrinsic accuracy of the *HST* guide-star coordinate system. The $H\alpha$ image (see Fig. 2) also shows the elongated ring structure with a peak in the north-northeastern corner at the position of the star clusters seen in the V - and I -band images. The $V-I$ colors of the clusters in the ringlike structure vary from 0.4 to 1.0, while a typical color outside and inside the ring is 1.5, reaching up to 1.9 in the dust lanes. Most of the dust is concentrated on the southeastern side of the elongated ringlike structure. Near-infrared high-resolution *HST* NICMOS observations of the nucleus will be reported in a future paper. They promise to shed more light on the issue of the true location of the nucleus in NGC 4038. Previous ground-based near-infrared imaging (Bushouse & Werner 1990; Hibbard et al. 2001; Mengel et al. 2001) does not have high enough spatial resolution to indicate the exact location of the nucleus.

The nucleus of NGC 4039, the southern component of the Antennae, is much easier to recognize in the V and I

images (see Fig. 3). Our identified nuclear position (the position of the optical peak) in Table 1 agrees to within about $2''$ of the estimated nuclear positions from the radio continuum data (Zhang et al. 2001) and near-infrared data (Mengel et al. 2001). The nucleus is surrounded by dust patches and dust lanes. There is also a minor peak of $H\alpha$ emission at the location of the nucleus, which could be due to continuum subtraction uncertainties. Much more intense $H\alpha$ emission is seen in the arm connecting to the nucleus. The $V-I$ color of the nucleus of NGC 4039 is about 1.0, and the surrounding area has a color around 1.3, with values of 1.7 in a dusty region close to the nucleus.

Neither NGC 4038 nor NGC 4039 is classified as a Seyfert or LINER nucleus. These nuclei are instead hosts of mild starbursts (e.g., Dahari 1985; Véron-Cetty & Véron 1986). Further evidence for the starburst nature of these nuclei comes from X-ray observations with the *ROSAT* High-Resolution Imager (Fabbiano et al. 1997) and with *Chandra* (Zezas et al. 2002a, 2002b). The northern X-ray nucleus (NGC 4038) has a soft spectrum, which hints at thermal emission and is probably related to a hot wind, whereas the thermal+power-law spectrum of the southern X-ray nucleus (NGC 4039) indicates a hot ISM and a contribution from X-ray binaries.

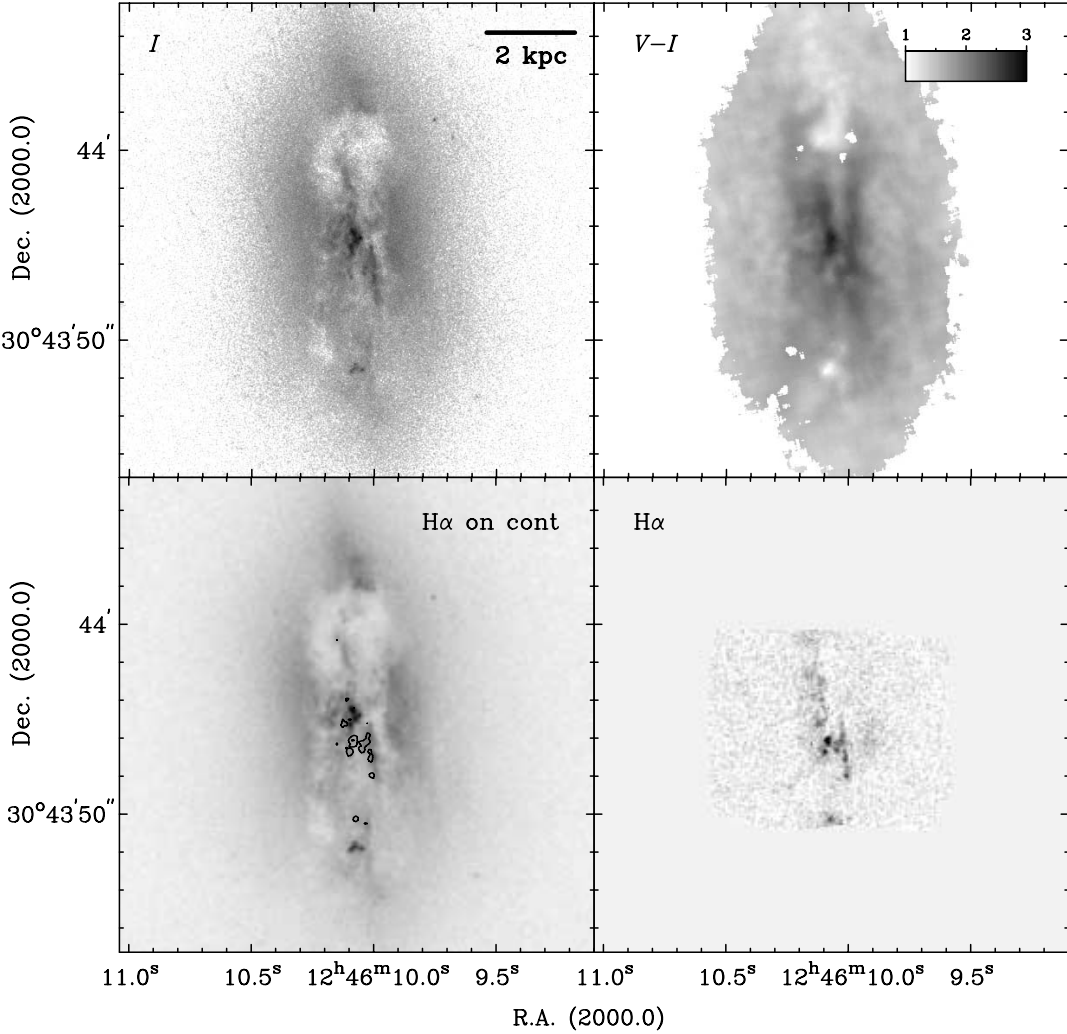


FIG. 4.—NGC 4676A, or Nuc 1, as in Fig. 2. This color index image and many of the subsequent color index images only show areas where the S/N was sufficiently high to reveal a meaningful, smooth color. The H α contour levels in the bottom left image are at 20% and 90% of 1.2×10^{-16} ergs s $^{-1}$ cm $^{-2}$ pixel $^{-1}$.

3.2. NGC 4676 (*The Mice*)

The Mice is a pair of spiral galaxies with only moderately active nuclei (classified as LINER-type by Keel et al. 1985). The nucleus of NGC 4676A, or Nuc 1 (the northern component of the pair), is covered by dust in our optical V and I images (Fig. 4). This dust is likely associated with the dense edge-on molecular disk imaged in CO(1–0) by Yun & Hibbard (2001). Adopting standard conversion factors, the observed peak CO flux density suggests that the nucleus of NGC 4676A is hidden beneath $A_V \sim 60$ mag of extinction.

Just south of the area of heavy dust obscuration near the base of the northern tail is a V-shaped structure (with the V being sideways and opening to the east, and the tip of the V at R.A. $12^{\text{h}}46^{\text{m}}10^{\text{s}}.1$ and decl. $30^{\circ}43'55.^{\prime\prime}0$) of brighter emission from young stellar clusters near the center of the main body. About $7''$ (3 kpc) to the south one can see a triangle-shaped structure of young clusters. In ground-based K' band imagery obtained by one of us (J. E. H.) the tip of the central V-shaped cluster is seen to lie near the peak emission (see also Bushouse & Stanford 1992), so we assume that the nucleus lies near this position. The H α emission from NGC 4676A is weak. In general, the emission is elongated in the

north-south direction of the main body. The V-shaped structure has very red $V-I$ colors above 2.2. Perhaps even more surprisingly, the color of the heavily extinguished dust patch near the base of the tail is actually *bluer* than its surroundings, having an average $V-I$ -value less than 1. We interpret this region as scattered light from young stars, which are mostly hidden by the dust. A hint of this young star population is seen in the V image (not shown here). Such a young star-forming region can be seen even more clearly in the new, deeper ACS images of the Mice (Ford et al. 2002). In contrast to the V-shaped structure, the triangle-shaped structure of clusters near the southern end of the main body has bluer colors than its surroundings, with $V-I$ -values around 1 or slightly below it.

The nucleus is easily identified in NGC 4676B, or Nuc 2. It is surrounded by a rather amorphous disk and a dust lane that seems to wrap around the whole disk, ending near the location of the nucleus (Fig. 5). There is a peak of H α emission offset by about $0''.2$ from the nucleus of NGC 4676B, but in general the H α emission is weak and patchy. The nucleus has $V-I$ colors close to 1.3. A dust patch near the nucleus has a $V-I$ color as red as 1.7. The majority of the disk outside the dust lanes and dust patches has a $V-I$

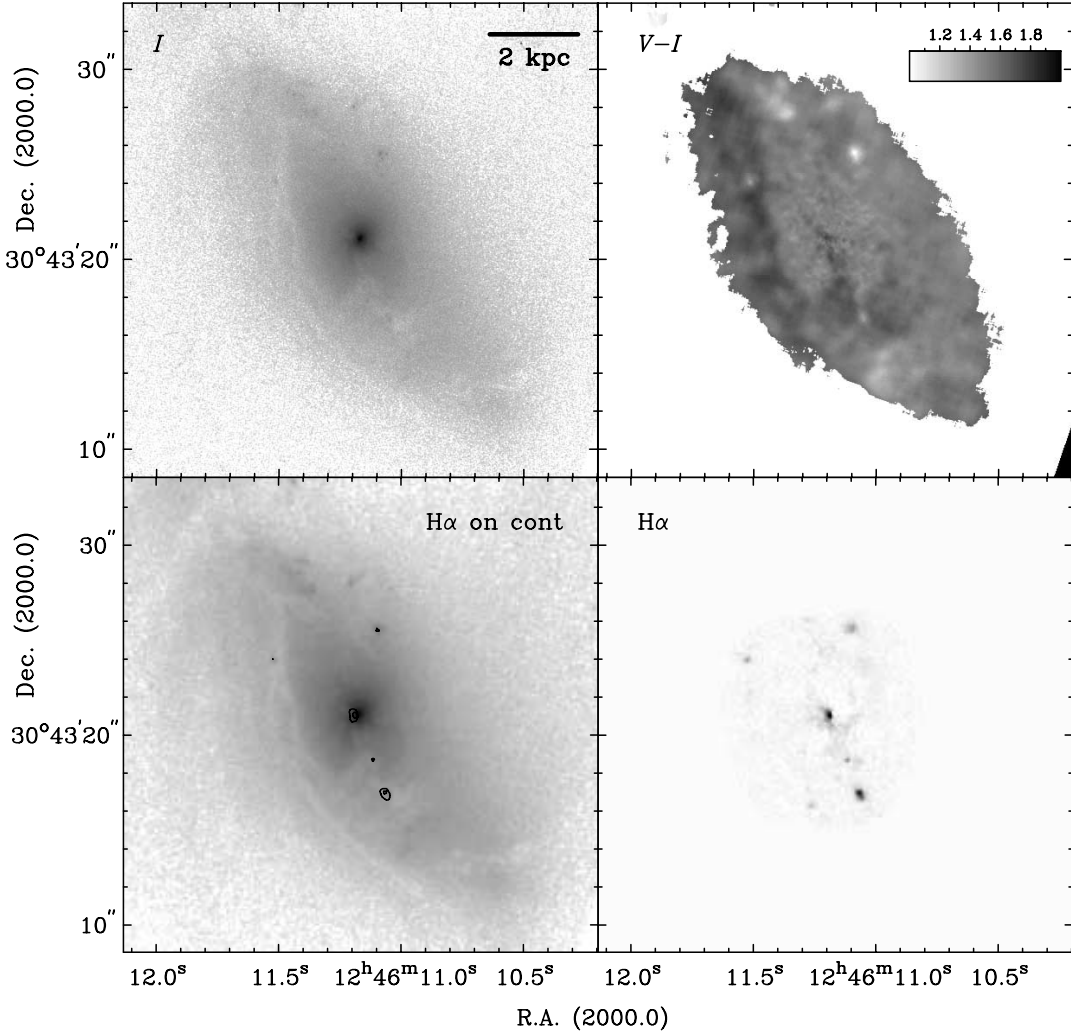


FIG. 5.—NGC 4676B, or Nuc 2, as in Fig. 2. The H α contour levels in the bottom left image are at 20% and 50% of 3.8×10^{-17} ergs s $^{-1}$ cm $^{-2}$ pixel $^{-1}$.

color of 1.2–1.3. The overall appearance of NGC 4676B, particularly the well-defined bulge/nucleus, is consistent with it being of an earlier Hubble type than its interacting partner, NGC 4676A (Yun & Hibbard 2001).

3.3. NGC 7592

This is the third most distant system in the Toomre sequence, and the main bodies of both galaxies fit within the PC chip of the WFPC2. NGC 7592A, or Nuc 1, further to the west, has an active Seyfert 2 nucleus, whereas NGC 7592B, or Nuc 2, is classified as a starbursting system (Dahari 1985; Rafanelli & Marziani 1992; Kewley et al. 2001; Hattori et al. 2002). NGC 7592A has a much better defined nucleus or bulge than NGC 7592B, consistent with the suggestion of Hattori et al. (2002), who argue that NGC 7592A is of an earlier Hubble type than NGC 7592B. Bushouse & Werner (1990) claim that NGC 7592A is seen almost face-on, because of its roundish appearance in ground-based optical and *K*-band images. If so, this galaxy appears to possess a barlike structure in the bulge, although the bar classification is uncertain because of patchy emission and one-sided dust. Similarly, Bushouse & Werner (1990) argued that NGC 7592B is more highly inclined to the line of sight. This, together with its later Hubble type, explains

why no clear nucleus is seen in this system. A comparison with the ground-based *K*-band image of Bushouse & Werner (1990) suggests that the nucleus of NGC 7592B lies near the center of the ringlike structure of bright clumps seen in Figure 6. We are not able to identify any specific clump with the nucleus.

The H α image shows abundant emission around the nucleus and the “bar” of NGC 7592A, and emission from the clumps in the ring of NGC 7592B, with a strong central depression in emission. The nucleus of NGC 7592A has blue colors, with $V-I$ around 0.8, contrasting to a dust lane lying on one side of the bar with a $V-I$ color close to 2.0. The southern side of the ring structure in NGC 7592B has very blue colors down to $V-I$ of 0.3, but there is a region of red colors of $V-I$ up to 1.9 in the northern part of the ring. Although there is dust visible at that location as well, the red color may suggest that the underlying red nucleus lies at this location.

3.4. NGC 7764A

This is the most distant system in our sample at $D = 122$ Mpc. The location of NGC 7764A in the Toomre sequence, among galaxies with clearly separate nuclei (Fig. 1) suggests that Toomre thought the nuclei of the two systems were still

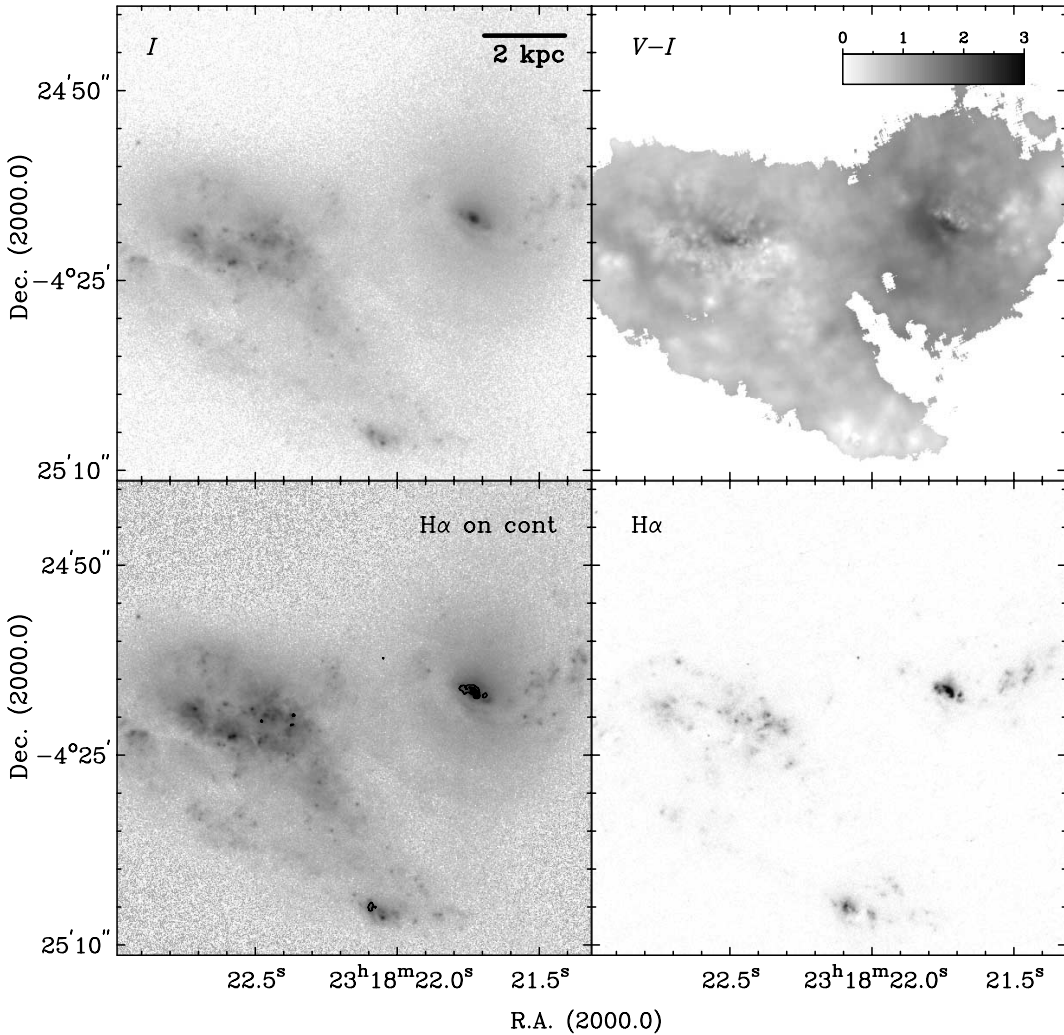


FIG. 6.—NGC 7592, as in Fig. 2. The $H\alpha$ contour levels in the bottom left image are at 10%, 30%, and 50% of $1.2 \times 10^{-15} \text{ ergs s}^{-1} \text{ cm}^{-2} \text{ pixel}^{-1}$.

distinct. However, our *HST* images (Fig. 7) do not obviously support the presence of two distinct nuclei. Future NICMOS near-infrared data will be critical in identifying the likely remains of the interacting galaxies. For now we only identify one main component from which both the tails are emanating. There is also a barred spiral galaxy, presumably at a similar redshift, displaced about $40''$ (23.7 kpc in projected distance) to the southeast of the main system (imaged on one of our WF chips; see Fig. 1), and a third system with apparent tidal streamers displaced about $40''$ to the northwest, just outside our PC image.

Our PC image reveals a shred or linear feature about $7''$ (4.1 kpc) to the northwest of the main body of NGC 7764A. About a dozen bright, blue ($V-I \sim 0.6-0.8$) star clusters lie within this filament. Between this filament and the center of Figure 7 is a very bright, very blue ($V-I \sim 0.22$) cluster. This cluster has associated $H\alpha$ emission with a “head-tail” morphology, with the cluster at the head and the tail pointing to the north-northeast. Following the head toward the center of the image in Figure 7, there is a string of $H\alpha$ regions crossed by dust lanes. The centermost $H\alpha$ region is weaker than the regions to its northwest and southeast, and is associated with two adjacent bright optical clusters. These two clusters lie near the region of very red colors in the $V-I$

map, with the reddest region ($V-I \sim 2.4$) associated with the eastern cluster. This strong dust concentration may indicate that this is the location of one of the nuclei. The western clump of the double cluster is bluer ($V-I \sim 1.5$) and brighter.

There are more bright $H\alpha$ regions about $3''$ (1.8 kpc) to the northeast of the double cluster associated with another bright star cluster embedded in dust. Further to the east of this is an amorphous luminous region with rather blue colors ($V-I \sim 0.6-0.8$).

3.5. NGC 6621 and NGC 6622

The northern component of this interacting galaxy pair, NGC 6621, has a dusty central region punctuated by patchy star clusters and ionized gas emission (Fig. 8). Two major dust lanes lead into the central region. One of them comes in from the northwest, following the long tidal tail at larger radii. The other dust lane intersects the nuclear region from the north, cutting a bright ridge of emission regions into two parts. $H\alpha$ emission is associated with the bright ridge of emission regions seen in the V and I images, and also with another emission patch across the dust lane coming in from the northwest. The emission ridge has $V-I$ colors around

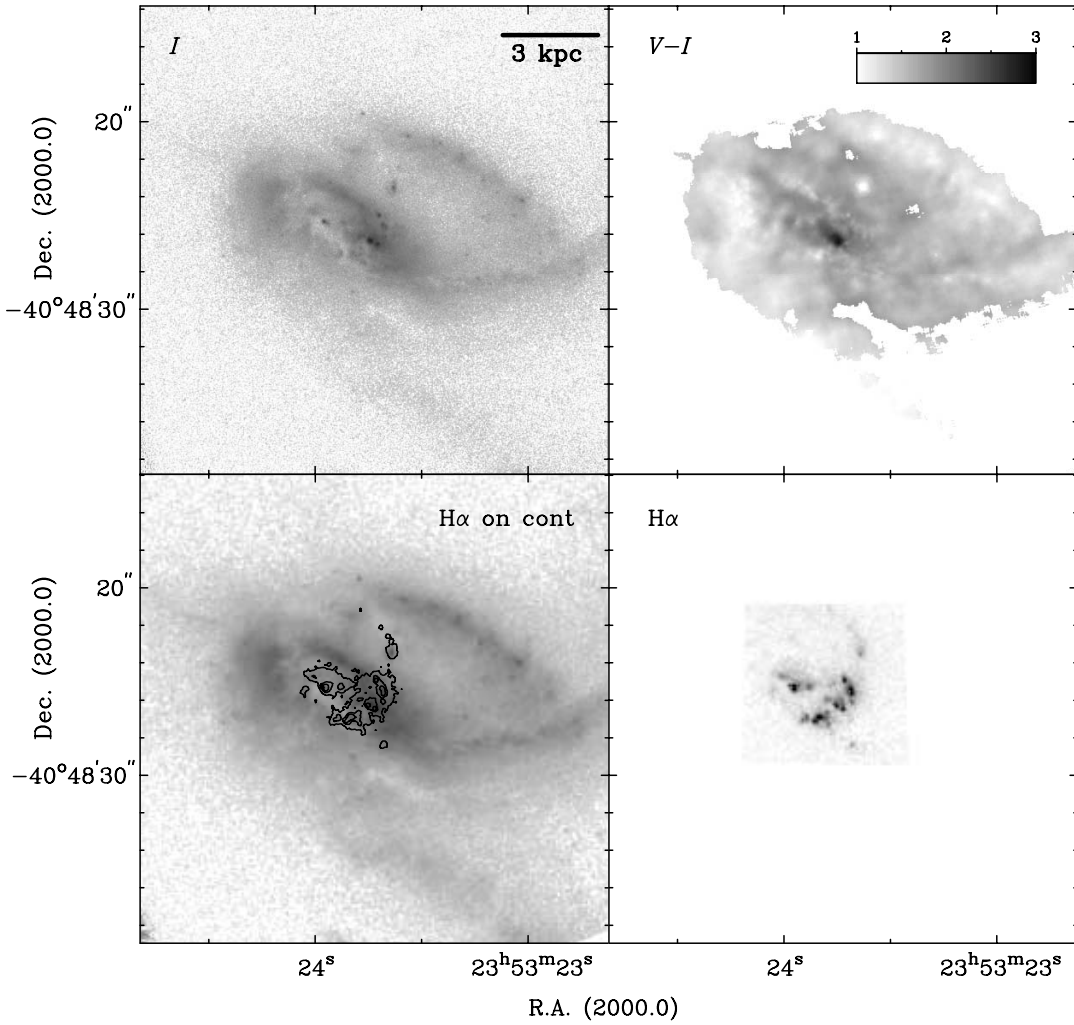


FIG. 7.—NGC 7764A, as in Fig. 2. The H α contour levels in the bottom left image are at 10%, 30%, and 50% of $2.4 \times 10^{-16} \text{ ergs s}^{-1} \text{ cm}^{-2} \text{ pixel}^{-1}$.

1.0, but in the surrounding dusty area the $V-I$ colors are as red as 2. The southwestern emission region across the dust lane from the emission ridge has a blue $V-I$ color of 0.5. The nuclear spectrum of NGC 6621 has been classified to be of starburst type (Veilleux et al. 1995). The ground-based near-infrared data of Bushouse & Werner (1990) show that the nucleus likely lies near the ridge of bright emission seen in our optical images, but it is not possible to constrain the true nuclear location from these images.

NGC 6622 has a well-defined nucleus and either a strong stellar bar or a close to edge-on orientation to the line of sight (Fig. 9). The J -band infrared image of Bushouse & Werner (1990) shows that the outer isophotes are not too far from being circular, making it unlikely that this is an edge-on galaxy. There is an obvious dust lane on the northern and northeastern side of the galaxy, most likely signifying perturbations caused by NGC 6621. There is practically no H α emission associated with NGC 6622, suggesting that it is an early Hubble-type galaxy. The nucleus and the bar have red $V-I$ colors up to 2.3. The typical color in the remainder of the disk is 1.3. There is a star-forming region in the area between NGC 6621 and NGC 6622, which has a blue $V-I$ color with typical values around 0.8 (*near top right edge*, Fig. 9).

3.6. NGC 3509

The second most distant galaxy of this sample, NGC 3509, falls in the middle of the Toomre sequence. The sketch of this system by Toomre (1977) suggests that he envisioned a large tail curving to the northwest and a shorter tail extending to the southwest. Deep ground-based CCD imagery obtained by one of us (J. E. H.) suggests that the southeastern feature is not a tail, but rather the bright ridge of an inclined disk. There is a very bright rectangular-shaped feature at the head of the southeastern feature, directly south of a central bulge (see also Arp 1966), which may have been interpreted as the bulge of the second system. Our *HST*/WFPC2 broadband imagery shows that this region resolves into a number of bright, blue stellar associations (Fig. 10), and we believe it is much more likely to be a collection of bright star-forming regions within the perturbed disk than the nucleus of a second system. The extremely blue colors of this region ($V-I$ colors around 0.5; the tip of this region is seen in Fig. 10, *bottom center*) are in spectacular contrast to the rest of the galaxy (typical $V-I$ values from 1.1 to 1.4) and indicate active star formation.

In our images we can clearly identify a single relatively undisturbed nucleus, surrounded by a swirl of dust lanes

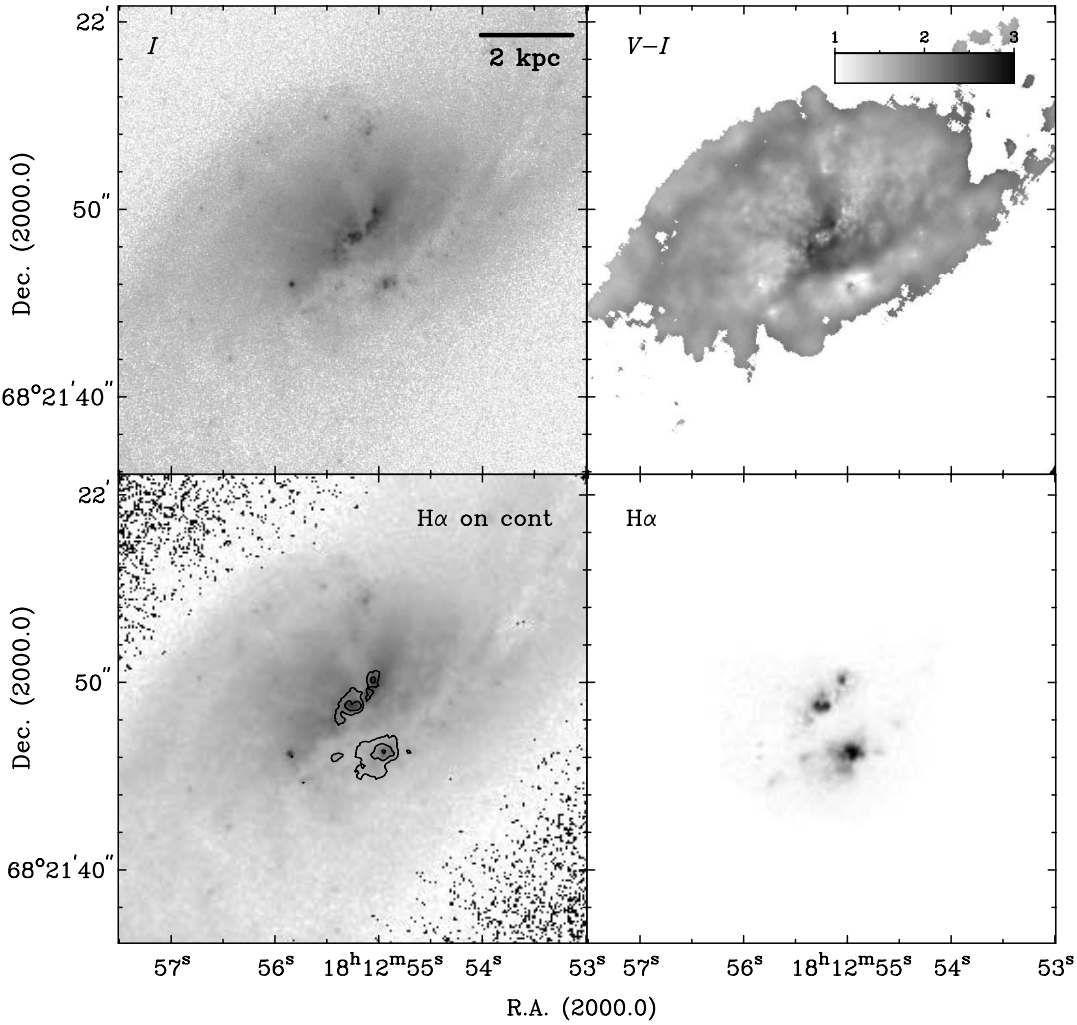


FIG. 8.—NGC 6621, as in Fig. 2. The H α contour levels in the bottom left image are at 5%, 20%, and 90% of 1.9×10^{-15} ergs s $^{-1}$ cm $^{-2}$ pixel $^{-1}$.

(center, Fig. 10). The H α image reveals a peculiar double-peaked H α structure straddling the nucleus in an orientation that is perpendicular to the main body of the nuclear region. H α emission, indicating ongoing star formation, is also seen in the blue region south of the nucleus.

In the absence of an obvious second tidal tail in the ground-based imagery, we find little evidence that NGC 3509 is the obvious result of a major disk-disk merger. It may instead be the result of a minor merger, or of an ongoing interaction with a smaller companion. In support of the minor merger hypothesis, we note the appearance of a roughly circular diffuse red concentration just to the north of the nucleus (12'', \sim 6 kpc; see Fig. 1, just off of the PC chip) which could be the remains of a smaller galaxy. In support of the interaction hypothesis, on a deep *R*-band CCD image taken by one of us (J. E. H.) we note the presence of a compact object lying \sim 2' toward southeast, along the minor axis of this system. This possible companion also has faint low surface brightness features pointing both toward and away from NGC 3509.

3.7. NGC 520

The southeastern component of NGC 520 is hidden behind a prominent and intricate dust lane (Fig. 11). This dust is likely associated with the dense edge-on molecular

disk imaged in CO (1–0) by Sanders et al. (1988b) and Yun & Hibbard (2001). Adopting standard conversion factors, the observed peak CO flux density suggests that the nucleus of NGC 520 is hidden beneath $A_V \sim 300$ mag of extinction. It is thus not surprising that the position of the primary nucleus is impossible to determine from our data. High-resolution future NICMOS observations may point out where this nucleus lies, but, judging from earlier ground-based near-infrared images (e.g., Bushouse & Stanford 1992; Kotilainen et al. 2001), the nucleus likely lies in the center of the heaviest dust absorption. Radio continuum images (e.g., Carral, Turner, & Ho 1990) show a disklike morphology coincident with the CO disk, suggesting ongoing star formation within the central molecular disk. Practically no H α emission is seen in our H α image at the position of the primary nucleus. Red $V-I$ colors are seen along most of the primary nucleus. However, at the location of the most dust-affected regions, as seen in the *I* image, we see relatively blue colors of 0.8 in the color index image. Again, as in the case of NGC 4676A, we interpret this as scattering of emission from young stars, hinted at in the *V*-band image (not shown here).

The secondary, northwestern nucleus (Fig. 12) comes presumably from an earlier Hubble-type disk galaxy that is now embedded within an extended atomic gas disk associated

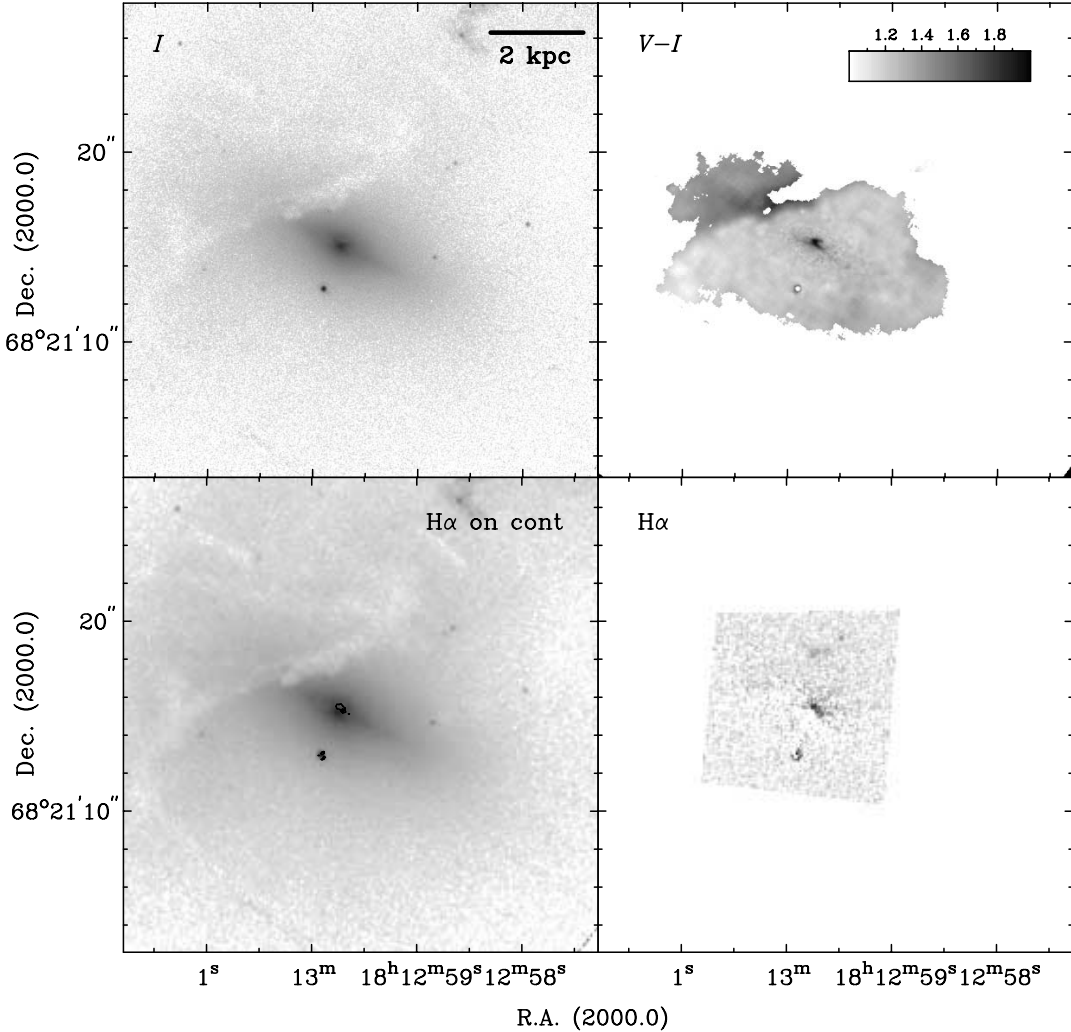


FIG. 9.—NGC 6622, as in Fig. 2. The H α contour level in the bottom left image is at 50% of 7.3×10^{-17} ergs s $^{-1}$ cm $^{-2}$ pixel $^{-1}$.

with the primary galaxy (Hibbard & van Gorkom 1996). The secondary nucleus is very well defined, although its surrounding disk seems to have been mostly disrupted in the merger and probably contributes now to the extended optical tails. The only significant H α emission near the secondary nucleus is in clumps within 1'' (150 pc) and displaced to the northwest. The secondary nucleus appears to have a bluish color, with $V-I$ of 0.6. This nucleus is observed to be in a poststarburst phase (Stanford & Balcells 1990, 1991; Bernlöhr 1993). The $V-I$ color toward the northwest of the nucleus has bluish values around 0.8, but dust reddens the color to 1.2 at about 3'' (450 pc) southeast of the nucleus.

3.8. NGC 2623

Consistent with its classification as a fairly advanced merger system, only one galaxy body is evident in NGC 2623 (Fig. 13). Again, based on the high spatial resolution optical *HST* images, it is impossible to tell the exact location of the nucleus or nuclei. A comparison with the *JHK* NICMOS images published by Scoville et al. (2000) suggests that the position of the brightest optical peak in the center of the main body of NGC 2623 is the true position of the nucleus, near J2000.0 coordinates of R.A. = 8 $^{\text{h}}38^{\text{m}}24^{\text{s}}.1$ and decl. = 25 $^{\circ}45'16''$. This nucleus is classified as a LINER by

Dahari (1985) and Vacci, Alonso-Herrero, & Rieke (1998). Dust surrounds the nucleus mostly on the southeastern, northern, and northwestern sides, although numerous dust lanes criss-cross the whole nuclear region (see Fig. 13).

A study by Joy & Harvey (1987) confirms the coalescence of two galaxies. Based on their near-infrared observations, they conclude that the merger is complete because only one nucleus is visible (which is surrounded by a single, symmetric nuclear region). This impression is confirmed by CO observations, which reveal a single centrally concentrated compact molecular disk with simple rotational kinematics (Bryant & Scoville 1999). There are also numerous young star clusters scattered around the main body and the surrounding shreds.

Most of the H α emission comes from a disk around the nuclear position and from a location north of the nucleus, but also from a position in the dust patch southeast of the nucleus. The nucleus has a very red $V-I$ color at 2.5, consistent with the reddish near-infrared colors found for the nucleus by Scoville et al. (2000). The red near-infrared $H-K$ color, together with a relatively large CO absorption index value (Ridgway, Wynn-Williams, & Becklin 1994), suggests that there has been a recent starburst in the nuclear region. The red colors continue for about 2'' (720 pc) to the north

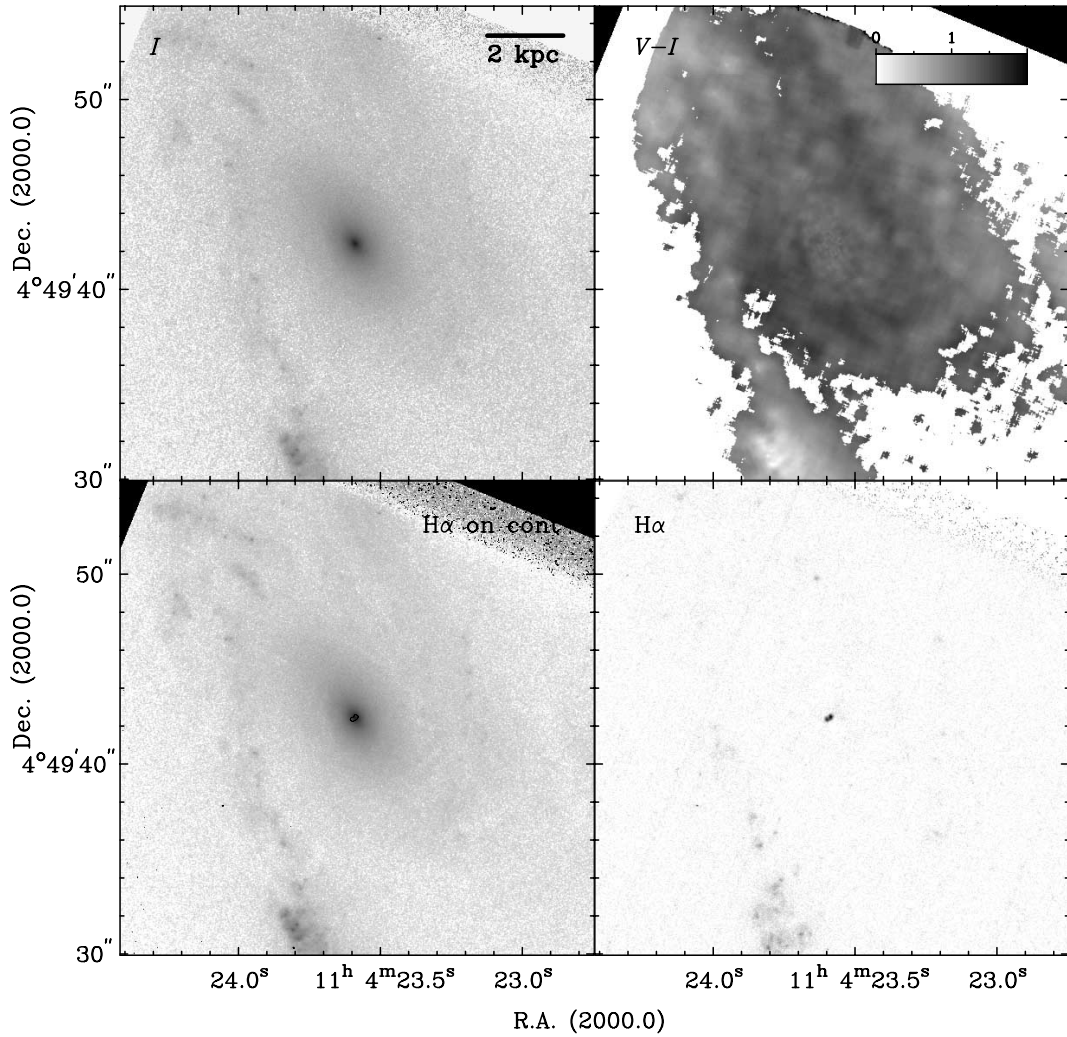


FIG. 10.—NGC 3509, as in Fig. 2. The H α contour level in the bottom left image is at 20% of 2.5×10^{-16} ergs s $^{-1}$ cm $^{-2}$ pixel $^{-1}$.

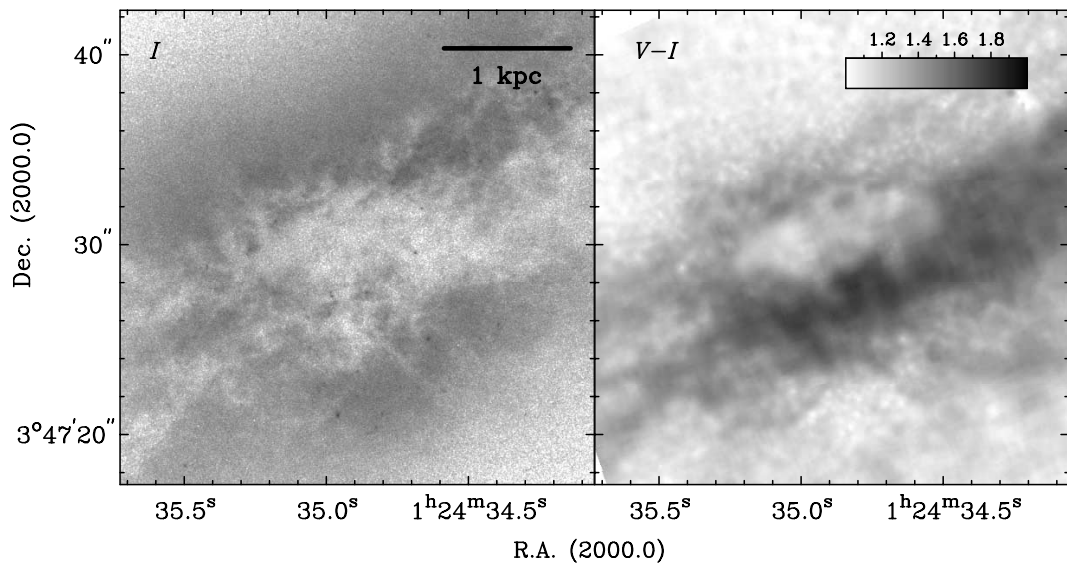


FIG. 11.—NGC 520 Nuc 1. *Left:* I image. *Right:* V-I image. The H α emission around the nucleus is not shown, as it is not significantly detected above the noise of the image.

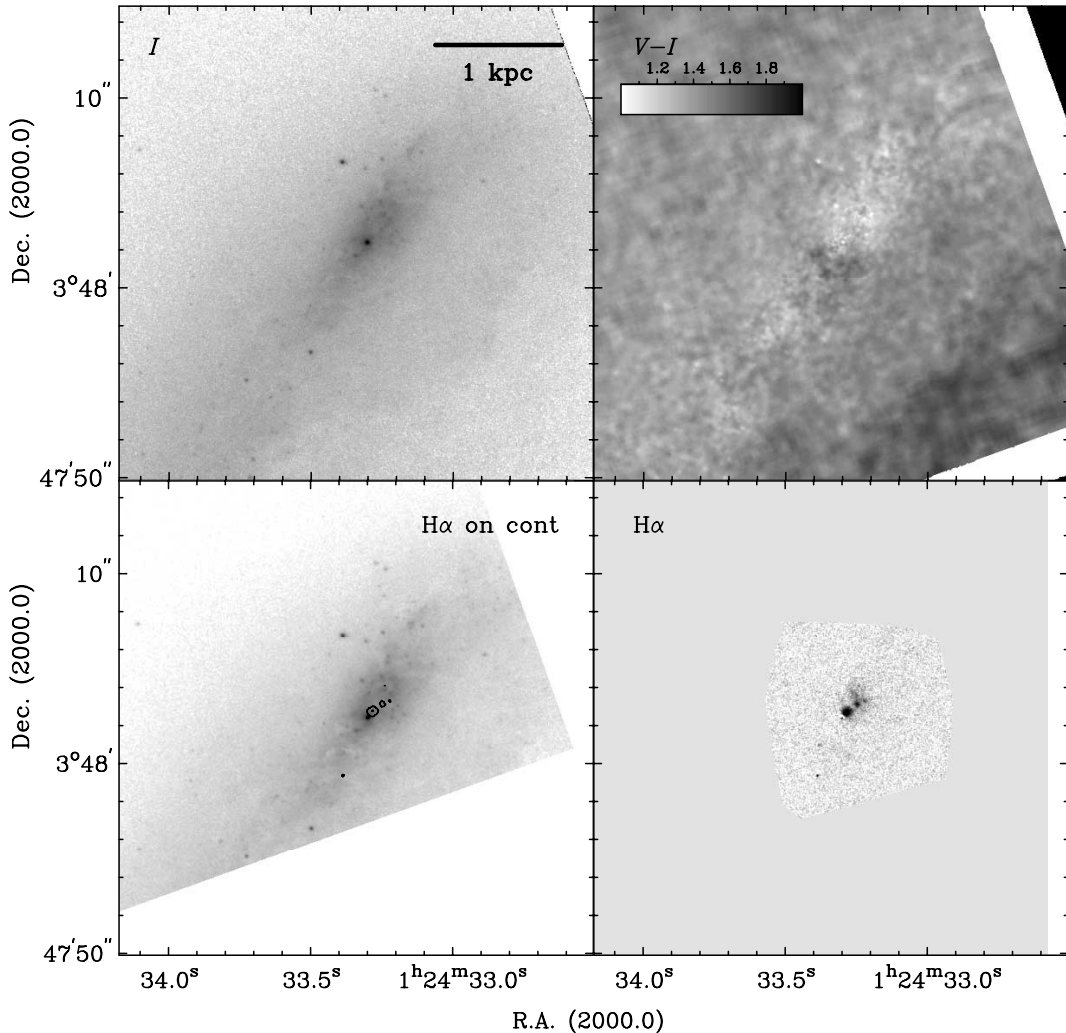


FIG. 12.—NGC 520 Nuc 2, as in Fig. 2. The $H\alpha$ contour levels in the bottom left image are at 20% and 90% of $1.4 \times 10^{-16} \text{ ergs s}^{-1} \text{ cm}^{-2} \text{ pixel}^{-1}$.

and northwest. The main body of NGC 2623 has $V-I$ colors close to 1.0 or just below it.

3.9. NGC 3256

Our optical *HST* images show one obvious nucleus located in the center of Figure 14 (see also Zepf et al. 1999). This nucleus is surrounded by a relatively symmetric spiral morphology. Near-infrared, radio continuum, and X-ray observations (e.g., Norris & Forbes 1995; Kotilainen et al. 1996; Lira et al. 2002) have discovered a second nucleus about $5''$ (885 pc) south of the primary nucleus (marked with an “X” in Fig. 14), presumably hidden beneath the dark (red) dust feature directly south of the primary nucleus in the $V-I$ image of Figure 14 (see also English et al. 2003). We do not see an optical source at the position of the second near-infrared, radio, and X-ray source. Our data therefore do not shed any new light on the nature of this source. Neither nucleus shows any evidence of being active. Studying the question of how many nuclei exist in this system (even three nuclei have been suggested by Lipari et al. 2000), would benefit from a detailed dynamical simulation of this merger system. The measurements for NGC 3256 in this paper refer only to the one nucleus we see in our WFPC2 images.

Archival NICMOS near-infrared images suggest that the position of the primary nucleus is close to the location of the brightest emission in our F814W image (Lipari et al. 2000). However, the optical *HST* images alone only show that this position is part of a ringlike structure, and there is nothing noticeably different about this location other than that it is the brightest clump in the image. Other bright regions are likely to be young star clusters or globular clusters, as reported by Zepf et al. (1999).

The $H\alpha$ emission is extended and follows the spiral structure, but the brightest emission occurs at the position of the primary nucleus. Most previous studies regard this nucleus to be of starburst type, although Véron-Cetty & Véron (1986) were unable to resolve its true nature. While the primary nucleus has a blue $V-I$ color near 0.7, the dusty region covering the secondary nucleus to the south of the primary nucleus has a $V-I$ color of 2.5 or redder. In contrast, the spiral arms visible in the V and I images have a blue $V-I$ color between 0.5 and 1.0.

3.10. NGC 3921

Only one nucleus is visible in NGC 3921 (Fig. 15). This galaxy is a postmerger system that has developed an

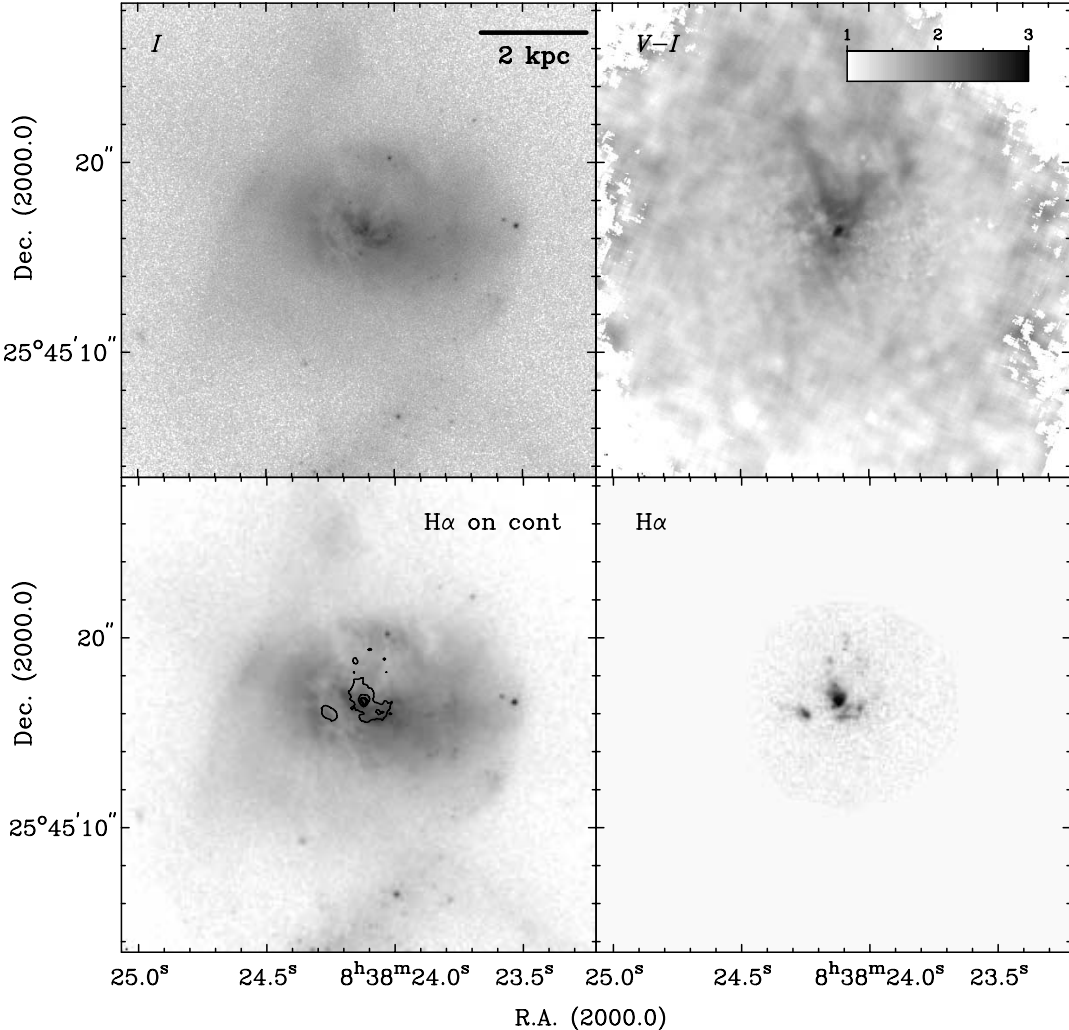


FIG. 13.—NGC 2623, as in Fig. 2. The $\text{H}\alpha$ contour levels in the bottom left image are at 10%, 50%, 80%, and 90% of $3.3 \times 10^{-16} \text{ ergs s}^{-1} \text{ cm}^{-2} \text{ pixel}^{-1}$.

elliptical-like central region (see, e.g., Schweizer 1996; Schweizer et al. 1996; Hibbard & Yun 1999), although numerous dust lanes still criss-cross this area (see Fig. 15). The evidence for a recent merger can be seen in the outer region where tails and plumes prevail (Hibbard & van Gorkom 1996). Several compact open star clusters or globular clusters can also be seen in the *HST* optical images kindly provided by B. Whitmore (see also Schweizer et al. 1996).

The $\text{H}\alpha$ emission is centered in a disk around the nucleus, but extends to larger radii. The nucleus is classified as a LINER by Stauffer (1982a, 1982b) and Dahari (1985). It lies in a location where the $V-I$ color gradient is very steep, as seen in the $V-I$ image, but the nucleus itself has normal values of $V-I$ around 1.1. To the southwest of the nucleus the $V-I$ color increases to ~ 1.8 at about $0''.5$ (190 pc) distance from the nucleus, and then it decreases and stays around 1.1–1.2 on that side of the galaxy. To the northeast the $V-I$ color decreases to values as low as 0.7 at about $0''.5$ from the nucleus, then stays around 0.9 for another $1''.5$ (570 pc). Dust extinction is at least partly responsible for this effect. Schweizer (1996) noticed that the nucleus lies substantially off center from the outer stellar isophotes of the main body.

3.11. NGC 7252 (*The Atoms for Peace Galaxy*)

We use the *HST* V and I images from Miller et al. (1997) to study the most advanced merger in the Toomre sequence. The remnant from the merger is probably between 0.5 and 1 Gyr old (Schweizer 1982; Hibbard & Mihos 1995). It has a single nucleus and is characterized by a $r^{1/4}$ profile typical of elliptical galaxies (Schweizer 1982; Miller et al. 1997; Hibbard & Yun 1999). It was quite a surprise, therefore, when *HST* revealed a central spiral disk (Miller et al. 1997 and Fig. 16). The disk extends to a radius of about $6''$ (1.8 kpc) and is therefore coincident with the molecular disk imaged by Wang et al. (1992). Our new *HST* $\text{H}\alpha$ image of this galaxy shows the disk to be actively forming stars, while the $V-I$ color map shows dust to be intertwined between the arms. In light of the results from recent hydrodynamical simulations (Barnes 2002) and the observation of tidal gas streaming back into the central regions of this remnant from the tidal tails (Hibbard et al. 1994; Hibbard & Mihos 1995), it seems likely that this central disk structure results from the reaccretion of tidally raised gas into the now relaxed central potential.

The nucleus appears resolved and is very bright, as we show in § 4. $\text{H}\alpha$ emission largely follows the spiral arms,

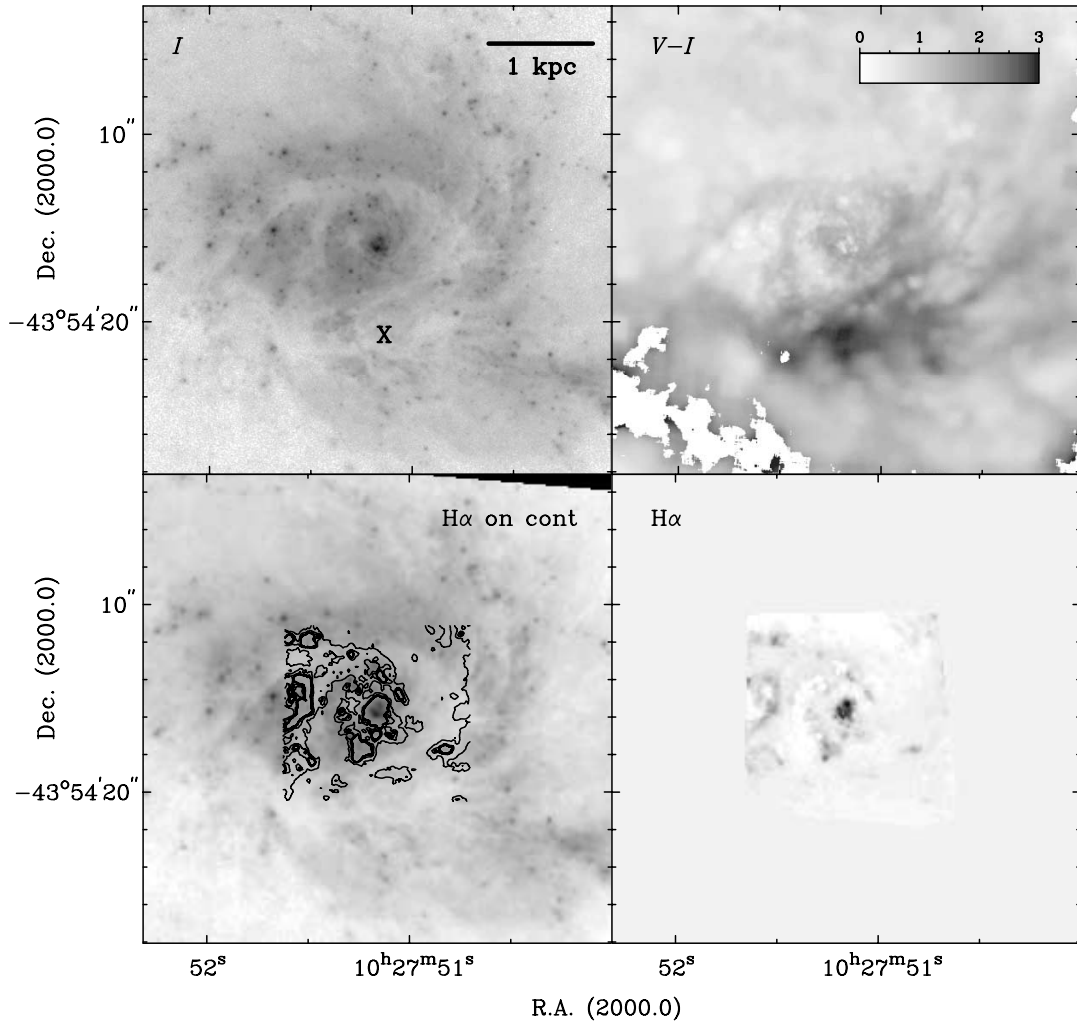


FIG. 14.—NGC 3256, as in Fig. 2. The location of the putative second nucleus is marked with an “X” in the top left panel. The $H\alpha$ contour levels in the bottom left image are at 10%, 50%, 80%, 90%, 95%, and 98% of $3.5 \times 10^{-16} \text{ ergs s}^{-1} \text{ cm}^{-2} \text{ pixel}^{-1}$.

although there appears to be a central $H\alpha$ source as well. However, our continuum subtraction, unfortunately, is uncertain in this area because of an optically very bright nucleus. Similarly, the central $V-I$ color is difficult to determine reliably because of the same problem, but the color there appears to be close to 1.3, whereas the surrounding spirals have $V-I$ colors as blue as 0.5.

Recent X-ray observations with *ASCA* revealed X-ray emission that can be described by a two-component model (Awaki et al. 2002), with soft emission ($kT = 0.72 \text{ keV}$), and a hard component ($kT > 5.1 \text{ keV}$). The hard component might indicate the existence of nuclear activity or even an intermediate-mass black hole.

4. CHANGE IN PHOTOMETRIC PROPERTIES WITH MERGER STAGE

We performed aperture photometry of the Toomre sequence galaxies to better understand the evolution of the nuclear region of merging galaxies. Because the isophotes in the nuclear region of merging galaxies are highly twisted, we did not attempt to fit ellipses and obtain radial surface brightness profiles. Instead, we performed aperture photometry within circular apertures, with radii of 100 pc

and 1 kpc. The lower value was dictated by the smallest resolvable physical scale in the most distant of our sample galaxies, whereas the upper value is somewhat arbitrary, but set because of our emphasis on the properties of the nuclear region. We have already characterized the morphology of the nuclear region at *HST* resolution in the individual galaxies above. Here we only report on the bulk photometric nuclear properties of each identified merger component galaxy.

Visual inspection of the images quickly reveals that none of the galaxies in the sample possess an extremely bright, pointlike active nucleus. Based on spectroscopic evidence, as cited in § 3, the only mildly active nuclei are in NGC 7592A (Seyfert 2), NGC 4676 Nuc 1 and Nuc 2 (LINER), NGC 2623 (LINER), and NGC 3921 (LINER). It is difficult to assess what the exact contribution of the nucleus to the integrated luminosities is.

The photometric measurements, converted to luminosity densities, are presented in Figures 17–19. The “merger stage,” plotted along the x -axis, refers to the original order of the sequence given by Toomre (1977), where 1 corresponds to NGC 4038/39 (the earliest merger stage) and 11 to NGC 7252 (the latest merger stage). The exact correspondence is given in the caption to Figure 17. Our observations do not

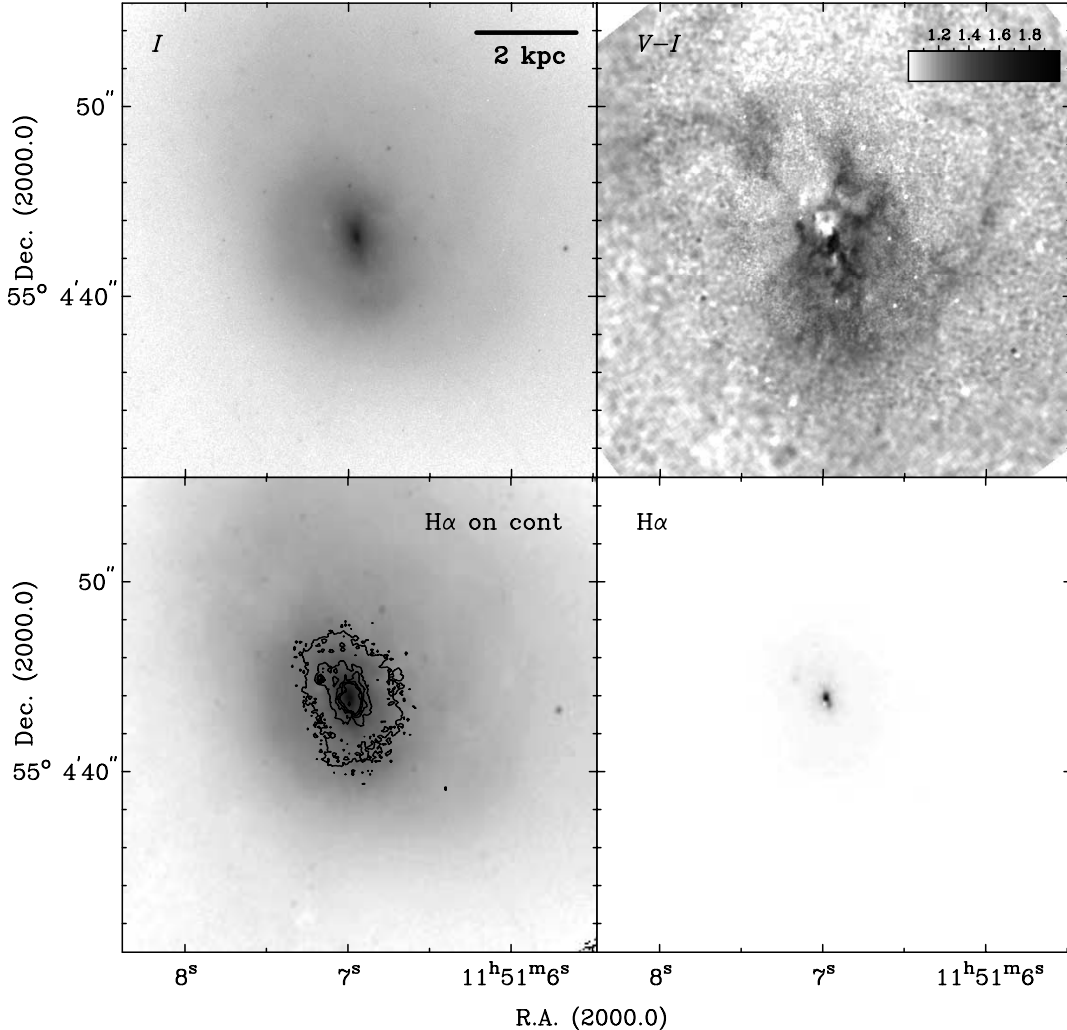


FIG. 15.—NGC 3921, as in Fig. 2. The $H\alpha$ contour levels in the bottom left image are at 10%, 30%, 50%, 70%, and 90% of $1.9 \times 10^{-16} \text{ ergs s}^{-1} \text{ cm}^{-2} \text{ pixel}^{-1}$.

suggest an obvious reordering of this sequence, although we are hampered by our inability to unambiguously identify all of the putative nuclei. Our tentative impression is that NGC 7764A (merger stage = 4) may be interacting with the disturbed galaxy lying off of our image, in which case it belongs near the beginning of the sequence. And NGC 3509 (merger stage = 6) is not an obvious merger at all. However, we will await NICMOS observations of this sequence before reaching any firm conclusions on this matter. We note that none of our conclusions will be affected if these two systems move earlier along or off of the sequence.

Apart from the large scatter in Figure 17 we see that the three latest merger stage systems (NGC 3256, 3921, and 7252) have the highest intrinsic luminosity densities. This is true for both apertures that we used (100 pc and 1 kpc). The range of luminosity density within 100 pc corresponds to a factor of more than 300. To a large extent this reflects the varying dust extinction in the central region, but partly also the morphology of the nuclear region (well-defined nuclei are bright, whereas components with no clearly recognizable nucleus are faint). With only $V-I$ colors available it is difficult to make a meaningful estimate of dust extinction. But, for example,

Figure 18 shows that in NGC 2623 the integrated $V-I$ color is very red within a 100 pc radius aperture, with a value around 2.2. Assuming that the true $V-I$ color is 1.4 (a more typical value seen in the same figure) would imply almost $A_V = 2$ mag of extinction with a typical extinction law of $A_\lambda \sim \lambda^{-1.85}$ (Landini et al. 1984). Since the extinction in the K band is only 1/10 of that in the V band, our future NICMOS images offer some hope of revealing the true location of the nucleus.

While the $V-I$ colors for the 100 pc aperture attain values anywhere between 0.8 and 2.4, the majority of the nuclei have rather typical colors for the centers of spiral nuclei and elliptical galaxies, ranging from 1.2 to 1.5 (see, e.g., Carollo et al. 1997). The presumably latest-stage merger, NGC 7252, has colors even bluer than normal ellipticals. However, the morphology of the dust lanes we see in the images suggests that dust obscuration is likely to be significant in many systems of the Toomre sequence.

The $H\alpha + [N II]$ luminosities (Fig. 19) show a marginal trend of increasing luminosities toward the late-stage mergers, most obviously in the largest 1 kpc aperture. However, the scatter is large, and based on the sample of 15 nuclei it is impossible to establish any definite trends.

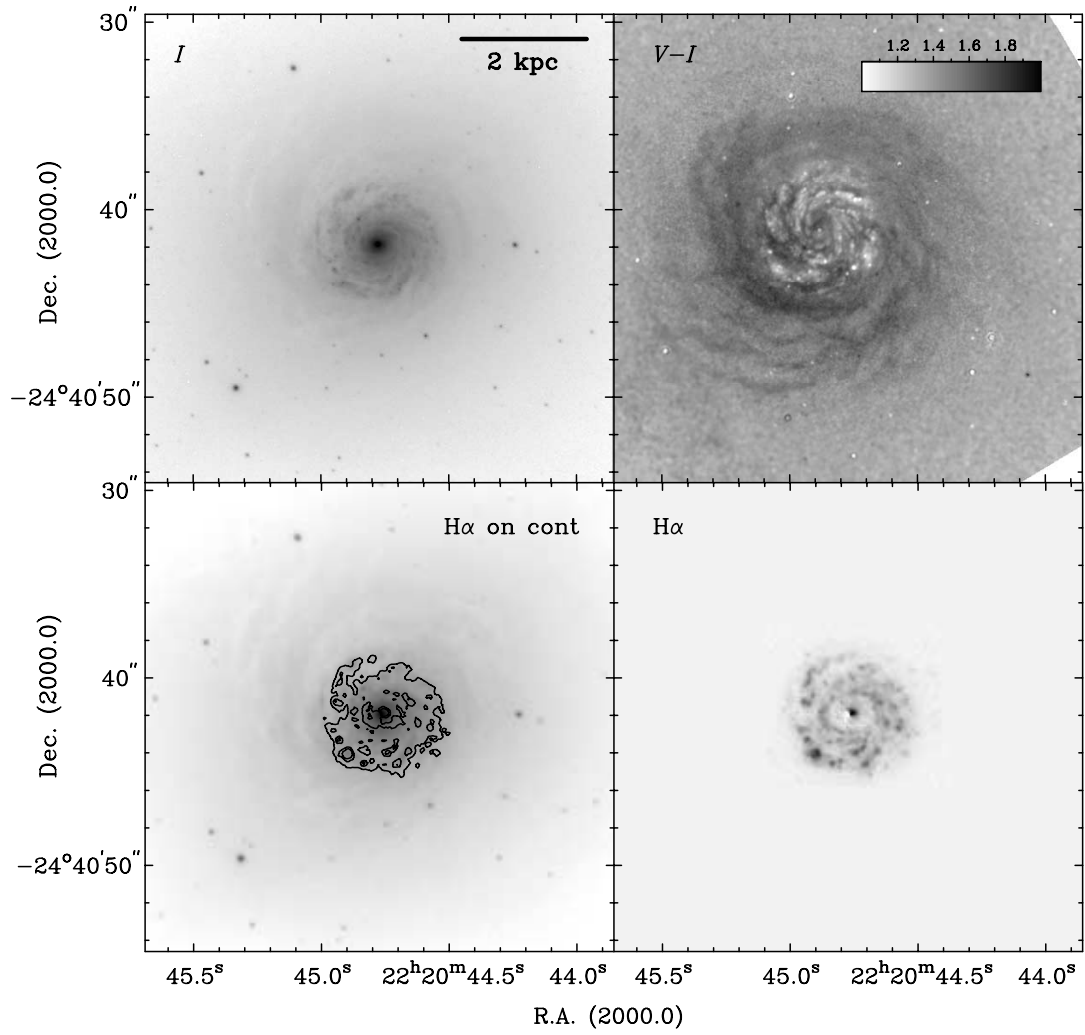


FIG. 16.—NGC 7252, as in Fig. 2. The H α contour levels in the lower left image are at 10%, 30%, and 50% of 7.2×10^{-16} ergs s $^{-1}$ cm $^{-2}$ pixel $^{-1}$.

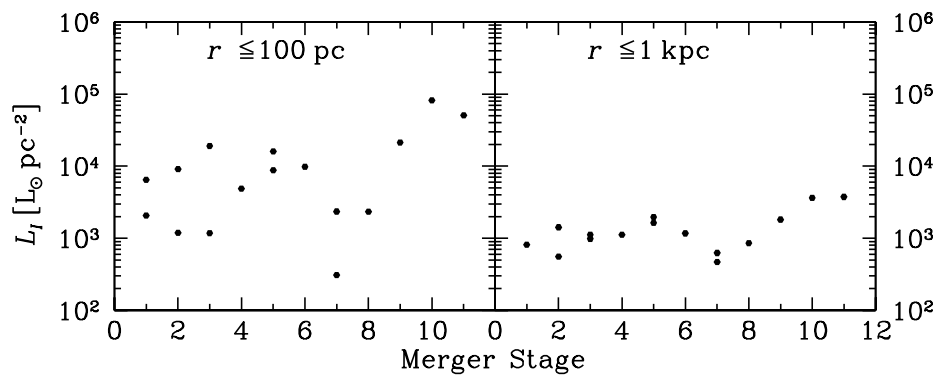


FIG. 17.—Circular I -band aperture photometry centered on the putative nucleus in each of the merging galaxies of the Toomre sequence. The horizontal axis represents the sequence as originally conceived by Toomre (1977). The merging stage numbers correspond to the individual galaxies as follows: (1) NGC4038/39; (2) NGC 4676; (3) NGC 7592; (4) NGC 7764A; (5) NGC 6621/22; (6) NGC 3509; (7) NGC 520; (8) NGC 2623; (9) NGC 3256; (10) NGC 3921; and (11) NGC 7252. The two-dimensional projected luminosity density is presented on the vertical axis, within apertures specified within the frame. *Left:* Within a 100 pc radius aperture; *right:* within a 1 kpc radius aperture. The luminosity densities have not been corrected for extinction. Uncertainties in the plotted values are smaller than the symbol size.

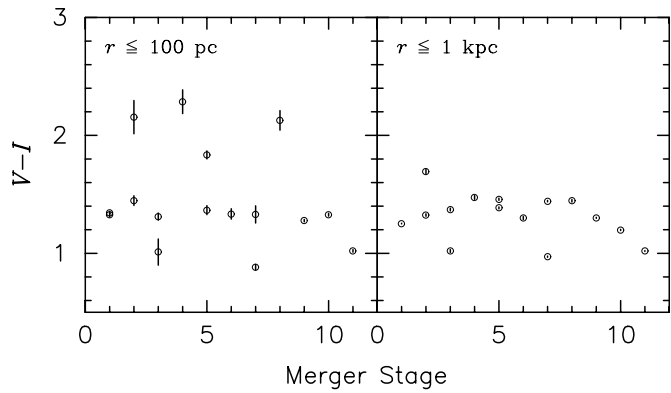


FIG. 18.—Integrated $V-I$ color indices within the circular apertures cited within the frames, as a function of the merger stage. The merger stage is defined as before in Fig. 17. The error bars are based on the combined errors in the V - and I -band aperture magnitudes, estimated using the standard propagation of error formulas.

Since mergers are expected to bring material into the center of galaxies and generate star formation there, we also study the nuclear concentration of light and line emission along the merging sequence. We measure the nuclear concentration quantitatively by taking the ratio of the luminosities within 100 pc to that within 1 kpc, for both the I band (Fig. 20) and the line emission (Fig. 21). We discuss the meaning of these ratios briefly in the following section.

5. DISCUSSION AND SUMMARY

The nuclear morphologies and central concentration are expected to be strongly affected by the timing and intensity of induced inflows and star formation during the merger. Numerical models of interacting galaxies have illustrated one mechanism by which interactions trigger these inflows and nuclear activity. Shortly after the galaxies first collide, the self-gravity of each disk amplifies the collisional perturbation into a growing $m = 2$ mode (Noguchi 1988; Barnes & Hernquist 1991; Mihos & Hernquist 1996). Depending on the structural properties of each galaxy, this mode can take

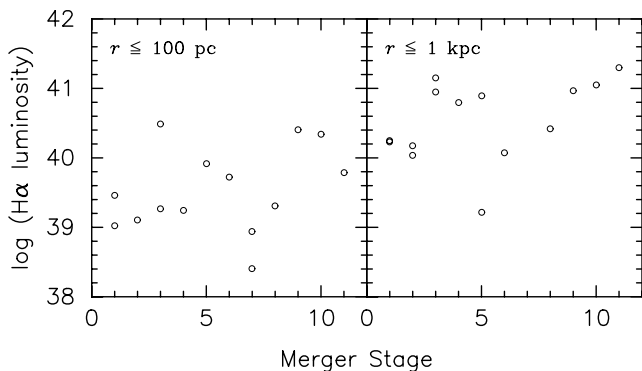


FIG. 19.—Integrated $\text{H}\alpha + [\text{N II}]$ luminosities in units of ergs per second within the circular apertures as cited within the frames, as a function of the merger stage. The merger stage is defined as before in Fig. 17. It was impossible to measure the flux within 1 kpc reliably for NGC 520 Nuc 2 (merger stage 7), since the galaxy was so close to the edge of the chip. Therefore, no 1 kpc luminosity is plotted here or in Fig. 21. Uncertainties in the fluxes are no better than 50%.

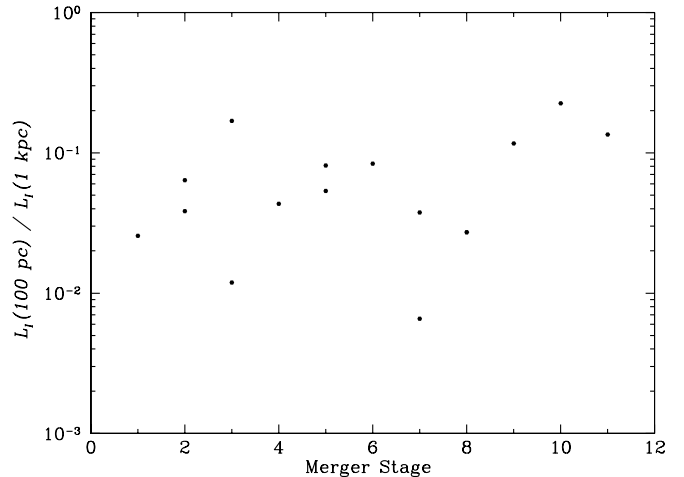


FIG. 20.—Ratio of the integrated I -band luminosity inside 100 pc to the integrated luminosity inside 1 kpc, plotted on a logarithmic scale, as a function of the merger stage.

the form of a strong bar, prominent spiral arms, or a pronounced oval distortion (Mihos & Hernquist 1996; Mihos, McGaugh, & de Blok 1997). These nonaxisymmetric structures drive shocks in the interstellar medium of the galaxies, leading to a spatial offset between the gaseous and stellar components, which robs the gas of angular momentum and can drive it inward well before the galaxies ultimately merge (Barnes & Hernquist 1991; Hernquist & Mihos 1995, 1996). The onset, strength, and duration of starbursts in interacting pairs can vary widely, depending on the properties of the host galaxies. Ultimately, however, any dynamical stability provided by the presence of a central bulge or diminished disk surface density will be overwhelmed by the strong gravitational torques and dissipative shocks during the final merging of the pair, at which point gaseous inflow and central activity should be ubiquitous. Once the coalescence of the galaxies is complete, the gravitational potential settles down and gas can settle into nuclear and/or spatially extended disks, supporting an extended period of relatively quiescent star formation.

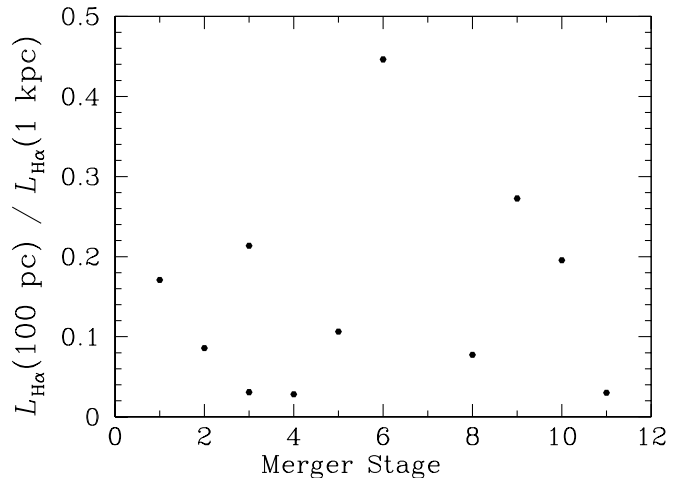


FIG. 21.—Ratio of the integrated $\text{H}\alpha + [\text{N II}]$ luminosity inside 100 pc to the integrated $\text{H}\alpha + [\text{N II}]$ luminosity inside 1 kpc, as a function of the merger stage. Uncertainties in the fluxes are no better than 50%.

Based on these kinds of models, we might expect to see an evolutionary trend for the nuclear properties of the Toomre sequence, from quiescent star formation in the early stages of the sequence to strong nuclear activity in the late stages. However, we see little evidence for such trends in the morphology, luminosity density, or colors of the stellar component, or in the morphology or intensity of the ionized gas emission, apart possibly from the fact that the latest-stage systems have some of the highest broadband luminosity densities and hints of starbursting central gaseous disk structures. This last suggestion is further strengthened by the trend toward bluer colors among the three latest-stage merger systems in Figure 18. A trend toward bluer colors was also seen in a study of merger remnants by van der Marel & Zurek (2000). Furthermore, the latest-stage merger systems have some of the highest nuclear H α luminosities (Fig. 19) and possess some of the largest concentrations of light in the central region (Fig. 20). Such a concentration is also seen to a certain extent in the H α +[N II] emission (Fig. 21).

Are our observations of the Toomre nuclei consistent with the broad picture of interaction-induced nuclear activity in galaxies evidenced in numerical simulations? In a broad sense, yes, although this consistency is mainly due to the variety of dynamical responses available to interacting systems. The late-stage mergers seem to have settled down, showing evidence for nuclear emission-line disks (NGC 2623, 3256, 3921, and 7252), more concentrated luminosity profiles and a trend toward bluer colors. Toomre sequence objects at earlier stages show very diverse properties, with no clear trends along the sequence. However, selecting a merging sequence based largely on the large-scale morphology of the tidal tails biases the sample toward a specific type of interaction—prograde interactions between disk galaxies—but not a specific type of disk galaxy. The galaxies that make up the Toomre sequence likely possess a variety of structural properties, so that there is no one-to-one correspondence between observed merger stage and nuclear morphology and activity. Put differently, the Toomre sequence is *not* a true evolutionary sequence on anything but the largest scales. Instead, it is composed of a variety of galaxies progressing down varied paths of interaction-driven activity. Expecting to discern a clear trend in nuclear properties is likely a naive hope.

Aside from the variety of physical conditions sampled by the Toomre nuclei, searching for trends along the Toomre sequence is also hampered by a number of observational concerns. First, the orientation of the galaxies with respect to the line of sight and to the orbital plane of the merger complicates the interpretation of the images. Second, extinction has a large effect on the observed morphologies, colors, and luminosities, as shown in § 4 (e.g., NGC 520 Nuc 1 and NGC 4676 Nuc 1). In this context, we hope to

improve upon the interpretation of the galaxy morphologies along the sequence through an analysis of NICMOS images of the entire Toomre sequence. These images will suffer from much less extinction and should also reveal the isophotes of the stellar population more clearly, thereby helping us in assessing the inclination of the merger components. The optical images shown here clearly demonstrate that dust in merging galaxies, even on small scales resolved by the *HST*, is not patchy enough to enable the identification of the true nuclei in optical bands.

In summary, these high-resolution WFPC2 images of the Toomre sequence have given us a detailed view of the nuclear regions of interacting and merging galaxies. We have characterized the broadband and emission-line morphologies of each member of the sequence, and measured the colors and luminosity densities of the nuclei. We find little evidence for clear trends in nuclear properties along the merger sequence, other than a suggestive rise in the nuclear luminosity density in the most evolved members of the sequence. The lack of clear trends in nuclear properties is likely due both to the effects of obscuration and geometry, as well as the physical variety of galaxies involved in the Toomre sequence. In subsequent papers we will combine our optical imaging with NICMOS imaging and STIS spectroscopy of the Toomre nuclei to give a detailed picture of the physical conditions in interacting and merging galaxies.

We are grateful to Brad Whitmore for providing us with fully reduced *HST* WFPC2 *V* and *I* images of NGC 3921, 4038/39, and 7252. We thank Nick Scoville for providing us with his adaptive filtering code. We are grateful to Zoltan Levay for help with the mosaicked images and thank William Keel for providing us with a copy of his *HST* image of NGC 6621/22 for help in planning our observations. We thank the anonymous referee for constructive comments that improved the clarity of the paper. Support for proposal 8669 was provided by NASA through a grant from the Space Telescope Science Institute, which is operated by the Association of Universities for Research in Astronomy, Inc., under NASA contract NAS5-26555. The research described in this paper was carried out in part by the Jet Propulsion Laboratory, California Institute of Technology, and was sponsored by the National Aeronautics and Space Administration. J. C. M. acknowledges support by the NSF through grant AST 98-76143 and by a Research Corporation Cottrell Scholarship. This research has made use of the NASA/IPAC Extragalactic Database, which is operated by the Jet Propulsion Laboratory, California Institute of Technology, under contract with the National Aeronautics and Space Administration. The LEDA database, operated by Centre de Recherche Astronomique de Lyon, is kindly acknowledged.

REFERENCES

- Arp, H. 1966, *Atlas of Peculiar Galaxies* (Pasadena: Caltech)
- Awaki, H., Matsumoto, H., & Tomida, H. 2002, ApJ, 567, 892
- Bahcall, J. N., Kirhakos, S., & Schneider, D. P. 1995, ApJ, 450, 486
- Barnes, J. E. 1988, ApJ, 331, 699
- . 1998, in Saas-Fee Advanced Course No. 26, *Galaxies: Interactions and Induced Star Formation*, ed. D. Friedli, L. Martinet, & D. Pfenniger (New York: Springer), 275
- . 2002, MNRAS, 333, 481
- Barnes, J. E., & Hernquist, L. 1991, ApJ, 370, L65
- . 1992, Nature, 360, 715
- . 1996, ApJ, 471, 115
- Bekki, K., & Couch, W. J. 2001, ApJ, 557, L19
- Bernlöhr, K. 1993, A&A, 270, 20
- Biretta, J. A., et al. 2000, WFPC2 Instrument Handbook, Version 5.0 (Baltimore: STScI)
- Borne, K. D., Bushouse, H., Lucas, R. A., & Colina, L. 2000, ApJ, 529, L77
- Bryant, P. M., & Scoville, N. Z. 1999, AJ, 117, 2632
- Bushouse, H. A., & Stanford, S. A. 1992, ApJS, 79, 213
- Bushouse, H. A., & Werner, M. W. 1990, ApJ, 359, 72
- Carollo, C. M., Franx, M., Illingworth, G. D., & Forbes, D. A. 1997, ApJ, 481, 710
- Carral, P., Turner, J. L., & Ho, P. T. P. 1990, ApJ, 362, 434
- Dahari, O. 1985, ApJS, 57, 643

- Dubinski, J., Mihos, J. C., & Hernquist, L. 1996, *ApJ*, 462, 576
- Duc, P. A., & Brinks, E. 2001, in *ASP Conf. Proc.* 240, *Gas and Galaxy Evolution*, ed. J. E. Hibbard, M. Rupen, & J. H. van Gorkom (San Francisco: ASP), 181
- Elmegreen, B. G., Kaufman, M., & Thomasson, M. 1993, *ApJ*, 412, 90
- English, J., Norris, R. P., Freeman, K. C., & Booth, R. S. 2003, *AJ*, 125, 1134
- Fabbiano, G., Schweizer, F., & Mackie, G. 1997, *ApJ*, 478, 542
- Ford, H. C., Illingworth, G. D., Clampin, M., & Hartig, G. (ACS Science Team and ESA). 2002, preprint (STScI-PRC02-11d)
- Georgakakis, A., Forbes, D. A., & Norris, R. P. 2000, *MNRAS*, 318, 124
- Hattori, T., Yoshida, M., Ohtani, H., Ishigaki, T., Sugai, H., Hayashi, T., Ozaki, S., & Ishii, M. 2002, *PASJ*, 54, 393
- Hernquist, L. 1992, *ApJ*, 400, 460
- Hernquist, L., & Mihos, J. C. 1995, *ApJ*, 448, 41
- . 1995, *AJ*, 110, 140
- Hibbard, J. E., Guhathakurta, P., van Gorkom, J. H., & Schweizer, F. 1994, *AJ*, 107, 67
- Hibbard, J. E., van der Hulst, J. M., Barnes, J. E., & Rich, R. M. 2001, *AJ*, 122, 2969
- Hibbard, J. E., & van Gorkom, J. H. 1996, *AJ*, 111, 655
- Hibbard, J. E., & Yun, M. S. 1999, *ApJ*, 522, L93
- Holtzman, J. A., Burrows, C. J., Casertano, S., Hester, J. J., Trauger, J. T., Watson, A. M., & Worthey, G. 1995, *PASP*, 107, 1065
- Hutchings, J. B., & Neff, S. G. 1992, *AJ*, 104, 1
- Joseph, R. D., & Wright, G. S. 1985, *MNRAS*, 214, 87
- Joy, M., & Harvey, P. M. 1987, *ApJ*, 315, 480
- Keel, W. C., Kennicutt, R. C., Jr., Hummel, E., & van der Hulst, J. M. 1985, *AJ*, 90, 708
- Kewley, L. J., Heisler, C. A., Dopita, M. A., & Lumsden, S. 2001, *ApJS*, 132, 37
- Kotilainen, J. K., Moorwood, A. F. M., Ward, M. J., & Forbes, D. A. 1996, *A&A*, 305, 107
- Kotilainen, J. K., Reunanen, J., Laine, S., & Ryder, S. D. 2001, *A&A*, 366, 439
- Landini, M., Natta, A., Oliva, E., Salinari, P., & Moorwood, A. F. M. 1984, *A&A*, 134, 284
- Lipari, S., Diaz, R., Taniguchi, Y., Terlevich, R., Dottori, H., & Carranza, G. 2000, *AJ*, 120, 645
- Lira, P., Ward, M. J., Zezas, A., Alonso-Herrero, A., & Ueno, S. 2002, *MNRAS*, 330, 259
- Lonsdale, C. J., Persson, S. E., & Matthews, K. 1984, *ApJ*, 287, 95
- Mengel, S., Lehnert, M. D., Thatte, N., Tacconi-Garman, L. E., & Genzel, R. 2001, *ApJ*, 550, 280
- Mihos, J. C., Bothun, G. D., & Richstone, D. O. 1993, *ApJ*, 418, 82
- Mihos, J. C., Dubinski, J., & Hernquist, L. 1998, *ApJ*, 494, 183
- Mihos, J. C., & Hernquist, L. 1994a, *ApJ*, 431, L9
- . 1994b, *ApJ*, 437, L47
- . 1996, *ApJ*, 464, 641
- Mihos, J. C., McGaugh, S. S., & de Blok, W. J. G. 1997, *ApJ*, 477, L79
- Miller, B. W., Whitmore, B. C., Schweizer, F., & Fall, S. M. 1997, *AJ*, 114, 2381
- Milosavljević, M., & Merritt, D. 2001, *ApJ*, 563, 34
- Neff, S. G., & Ulvestad, J. S. 2000, *AJ*, 120, 670
- Noguchi, M. 1988, *A&A*, 201, 37
- Norris, R. P., & Forbes, D. A. 1995, *ApJ*, 446, 594
- Quinlan, G. D., & Hernquist, L. 1997, *NewA*, 2, 533
- Quinlan, G. D., Hernquist, L., & Sigurdsson, S. 1995, *ApJ*, 440, 554
- Rafanelli, P., & Marziani, P. 1992, *AJ*, 103, 743
- Read, A. M., & Ponman, T. J. 1998, *MNRAS*, 297, 143
- Ridgway, S. G., Wynn-Williams, C. G., & Becklin, E. E. 1994, *ApJ*, 428, 609
- Sanders, D. B., Scoville, N. Z., Sargent, A. I., & Soifer, B. T. 1988b, *ApJ*, 324, L55
- Sanders, D. B., Soifer, B. T., Elias, J. H., Madore, B. F., Matthews, K., Neugebauer, G., & Scoville, N. Z. 1988a, *ApJ*, 325, 74
- Schweizer, F. 1982, *ApJ*, 252, 455
- . 1990, in *Dynamics and Interactions of Galaxies*, ed. R. Wielen (Heidelberg: Springer), 60
- . 1996, *AJ*, 111, 109
- . 1998, in *Galaxies: Interactions and Induced Star Formation*, Saas-Fee Advanced Course 26, ed. D. Friedli, L. Martinet, & D. Pfenniger (New York: Springer), 105
- Schweizer, F., Miller, B. W., Whitmore, B. C., & Fall, S. M. 1996, *AJ*, 112, 1839
- Scoville, N. Z., et al. 2000, *AJ*, 119, 991
- Springel, V., & White, S. D. M. 1999, *MNRAS*, 307, 162
- Stanford, S. A., & Balcells, M. 1990, *ApJ*, 355, 59
- . 1991, *ApJ*, 370, 118
- Stanford, S. A., & Bushouse, H. A. 1991, *ApJ*, 371, 92
- Stauffer, J. R. 1982a, *ApJ*, 262, 66
- . 1982b, *ApJS*, 50, 517
- Surace, J. A., Sanders, D. B., & Evans, A. S. 2001, *AJ*, 122, 2791
- Toomre, A. 1977, in *The Evolution of Galaxies and Stellar Populations*, ed. B. M. Tinsley & R. B. Larson (New Haven: Yale Univ. Press), 401
- Toomre, A., & Toomre, J. 1972, *ApJ*, 178, 623
- Vacci, L., Alonso-Herrero, A., & Rieke, G. H. 1998, *ApJ*, 504, 93
- van der Marel, R. P., et al. 2003, in preparation
- van der Marel, R. P., & Zurek, D. 2000, in *ASP Conf. Ser.* 197, *Dynamics of Galaxies: From the Early Universe to the Present*, ed. F. Combes, G. A. Mamon, & V. Charmandaris (San Francisco: ASP), 323
- Veilleux, S., Kim, D.-C., Sanders, D. B., Mazzarella, J. M., & Soifer, B. T. 1995, *ApJS*, 98, 171
- Verdoes Kleijn, G. A., Baum, S. A., de Zeeuw, P. T., & O'Dea, C. P. 1999, *AJ*, 118, 2592
- Véron-Cetty, M.-P., & Véron, P. 1986, *A&AS*, 66, 335
- Wang, Z., Schweizer, F., & Scoville, N. Z. 1992, *ApJ*, 396, 510
- Weedman, D. 1983, *ApJ*, 266, 479
- Whitmore, B. C., Miller, B. W., Schweizer, F., & Fall, S. M. 1997, *AJ*, 114, 1797
- Whitmore, B. C., & Schweizer, F. 1995, *AJ*, 109, 960
- Whitmore, B. C., Zhang, Q., Leitherer, C., Fall, S. M., Schweizer, F., & Miller, B. W. 1999, *AJ*, 118, 1551
- Young, P. J. 1980, *ApJ*, 242, 1232
- Yun, M. S., & Hibbard, J. E. 2001, *ApJ*, 550, 104
- Zepf, S. E., Ashman, K. M., English, J., Freeman, K. C., & Sharples, R. M. 1999, *AJ*, 118, 752
- Zezas, A., Fabbiano, G., Rots, A. H., & Murray, S. S. 2002a, *ApJ*, 577, 710
- . 2002b, *ApJS*, 142, 239
- Zhang, Q., Fall, S. M., & Whitmore, B. C. 2001, *ApJ*, 561, 727
- Zwicky, F. 1950, *Experientia*, 6, 441
- . 1956, *Ergeb. Exakten Naturwiss.*, 29, 344
- . 1964, *ApJ*, 140, 1467